




Theory of Valley Splitting in Si/SiGe Spin-Qubits: Interplay of Strain, Resonances and Random Alloy Disorder

Abel Thayil ^{*}, Lasse Ermoneit , and Markus Kantner [†]

Weierstrass Institute for Applied Analysis and Stochastics (WIAS), Mohrenstr. 39, 10117 Berlin, Germany

Electron spin-qubits in silicon-germanium (SiGe) heterostructures are a major candidate for the realization of scalable quantum computers. A critical challenge in strained Si/SiGe quantum wells (QWs) is the existence of two nearly degenerate valley states at the conduction band minimum that can lead to leakage of quantum information. To address this issue, various strategies have been explored to enhance the valley splitting (*i.e.*, the energy gap between the two low-energy conduction band minima), such as sharp interfaces, oscillating germanium concentrations in the QW (known as wiggle well) and shear strain engineering. In this work, we develop a comprehensive envelope-function theory augmented by empirical nonlocal pseudopotential theory to incorporate the effects of alloy disorder, strain, and non-trivial resonances arising from interaction between valley states across different Brillouin zones. We apply our model to analyze common epitaxial profiles studied in the literature with a focus on wiggle well type structures and compare our results with previous work. Our framework provides an efficient tool for quantifying the interplay of these effects on the valley splitting, enabling complex epitaxial profile optimization in future work.

I. INTRODUCTION

Electron spin-qubits in Si/SiGe quantum dots (QDs) are one of the major candidates for the realization of fault-tolerant universal quantum computers [1–3]. The material platform has excellent scalability prospects because of the abundance of nuclear spin free isotopes (*e.g.*, ^{28}Si and ^{76}Ge) required for long coherence times and its compatibility with industrial fabrication technology [4–6]. Experiments have demonstrated high-fidelity state initialization and readout in combination with one and two-qubit gates exceeding the fault-tolerance threshold [7–9]. Scalable quantum computing architectures require coherent coupling of distant qubits to overcome crosstalk and qubit wiring limitations [10, 11]. As a major step in this direction, coherent qubit transfer across the chip was recently demonstrated using conveyor-mode electron spin-qubit shuttles [12–14].

One of the key challenges in the design of reliable Si/SiGe qubits is the enhancement of the energy splitting between the two nearly degenerate valley states at the conduction band minimum of a biaxially strained SiGe/Si/SiGe quantum well (QW), see Fig. 1. The energy splitting between these states, called *valley splitting*, is caused by the coupling of the two valley states by the heterostructure potential [15–17]. Interface roughness and random alloy disorder in the SiGe barrier [18–20] cause the valley splitting to fluctuate across the chip with typical values ranging from several tens to hundreds of μeV [21–24]. These statistical fluctuations of the valley splitting are notoriously difficult to control and inevitably lead to spatial domains with very low splitting, where it becomes comparable with the Zeeman-splitting [23, 25, 26]. As a result, low valley splittings lead to so-called *spin-valley*

hotspots, which are a potential source for spin-dephasing and leakage of quantum information [27, 28]. While these issues might be secondary for stationary qubits, they are particularly critical in spin-qubit shuttles, where the electron is conveyed over micrometer distances across a disordered landscape [29, 30]. For such applications a reliably large valley splitting above 200 μeV would be desirable to avoid spin-valley hotspots [29, 31, 32].

Recently, several heuristic strategies have been proposed to enhance the valley splitting by engineering the Si/SiGe heterostructure [19, 31, 33, 34]. These include sharp interfaces, narrow QWs and QWs with uniform low Ge-concentration [18] and more elaborate epitaxial profiles in the QW such as a Ge-spike [35] or an oscillating Ge concentration, known as the *wiggle well* [31, 33, 34]. In all these concepts, there is a complex interplay of resonances, strain and disorder effects, which can lead to an enhancement of the mean valley splitting. For practical applications, however, it is important to assess the magnitude of the deterministic enhancement along with the strength of the disorder-induced fluctuations.

The theoretical description of valley splitting is primarily based on effective mass models, partially augmented by empirical tight-binding models [18, 19, 33, 36, 37], pseudopotential theory [31, 38] or density functional theory [16, 17, 39]. Moreover, these effective mass models have also been combined with statistical models to incorporate the effects of alloy disorder. For instance, in Refs. [18–20] alloy fluctuations have been modeled by sampling of Ge atoms in the primitive unit cells of the crystal from a (scaled) binomial distribution. Alternatively, there are also approaches in which the alloy disorder is already taken into account at the level of the electronic band structure [31]. Furthermore, the coupling between valley states across different Brillouin zones is inconsistently accounted for in the literature. These effects lead to non-trivial resonances, that are addressed in several studies [31, 33, 34], whereas most of the existing literature employs the so-called “ $2k_0$ -theory”, where only the direct interaction of

^{*} thayil@wias-berlin.de

[†] kantner@wias-berlin.de

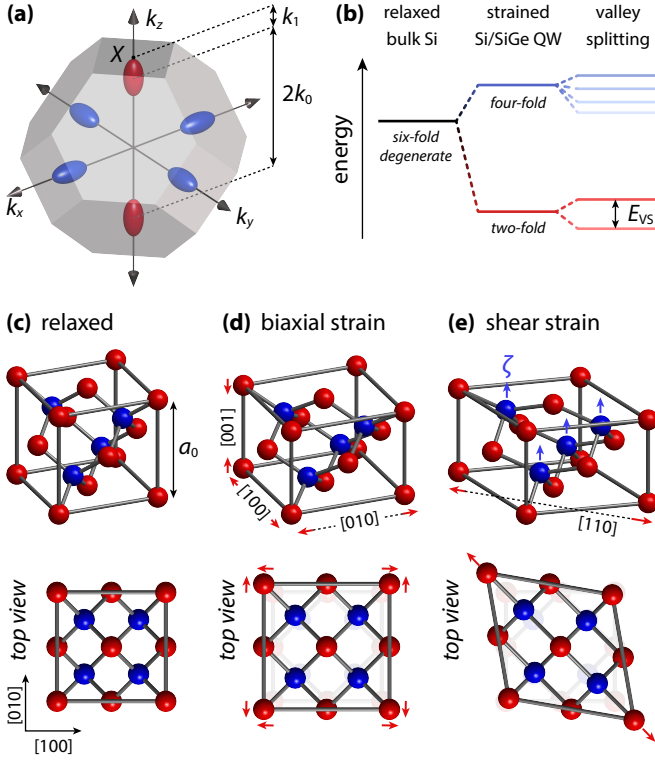


Fig. 1. (a) First Brillouin zone of the face-centered cubic (fcc) lattice. The degeneracy between the six equivalent conduction band minima in Si near the X-points is lifted by strain. (b) Energy diagram for the conduction band ground states in Si/SiGe quantum dots. Biaxial strain due to lattice mismatch between Si and SiGe leads to a separation of the two valleys oriented along $[001]$ and $[00\bar{1}]$ from the other four conduction band ground state valleys. The heterostructure potential and alloy disorder finally lift the remaining degeneracies. (c) Cubic unit cell of relaxed bulk Si (diamond crystal) composed of two interpenetrating fcc sub-lattices separated by a non-primitive translation along a quarter of the face diagonal. Atoms of the first and second fcc sub-lattice are shown in red and blue, respectively. (d) Biaxial strain along $[100]$ and $[010]$ yields a tetragonal crystal with reduced symmetry. Similar to the relaxed crystal, the two sub-lattices are interchangeable by a nonsymmorphic screw symmetry [31, 33]. (e) Additional shear strain along $[110]$ further reduces the symmetry to an orthorhombic system. The displacement between the two sub-lattices is controlled by Kleinman's internal ionic displacement parameter ζ (blue arrows). The nonsymmorphic screw symmetry, which maps the two sub-lattices onto each other, is broken by the shear strain.

the two valley states within the same Brillouin zone is considered [15, 19, 20, 27, 40, 41]. Finally, only few works explicitly discuss the impact of strain [33, 36, 42, 43]. In particular, merely the recent paper by Woods *et al.* [33] provides a combined analysis of non-trivial resonances and (shear) strain based on an effective mass theory derived from a tight-binding model. This model, however, disregards disorder-induced enhancements of the valley splitting.

In order to improve the understanding of the complex

physics determining the valley splitting in Si/SiGe qubits, it is pertinent to develop a comprehensive theoretical model that combines all of the aforementioned effects – namely strain, random alloy disorder and non-trivial resonances – into a unified framework. This objective has been accomplished in the present paper by means of an effective mass model, which merges several existing concepts consistently in a common framework. We demonstrate that our model faithfully reproduces several known results on valley splitting statistics, interface effects and the shear strain-dependency of the long-period wobble well, but also extends the state of the art.

The paper is organized as follows: In Sec. II, we provide the theoretical model for the valley-splitting in Si/SiGe QDs which involves a multi-valley coupled envelope equation, a statistical model of the random alloy disorder and the empirical pseudopotential method to account for the electronic band structure, strain and crystal symmetries. We provide expressions for the statistical properties of the valley splitting. Numerical results are described in Sec. III. Major attention is devoted to strain-induced effects, which extend previous findings on the QW interface-width dependency and wobble well-type heterostructures. Finally, Sec. IV provides a thorough discussion of the results and a comparison with similar models followed by an outlook in Sec. V. Several technical considerations on the derivation of the multi-valley coupled envelope equation model, band structure coefficients and valley splitting statistics can be found in the appendix.

II. VALLEY SPLITTING THEORY

A. Coupled Envelope Equations

The interaction of the two nearly degenerate low-energy valley states at the conduction band minimum $\mathbf{k} = \pm\mathbf{k}_0 \approx (0, 0, \pm 0.84) \times 2\pi/a_0$ of a biaxially (tensile) strained QW grown in $[001]$ direction is described by the coupled envelope equation model [16, 31, 33]

$$\begin{pmatrix} H_0(\mathbf{r}) & V_c(\mathbf{r}) \\ V_c^*(\mathbf{r}) & H_0(\mathbf{r}) \end{pmatrix} \begin{pmatrix} \Psi_+(\mathbf{r}) \\ \Psi_-(\mathbf{r}) \end{pmatrix} = E \begin{pmatrix} \Psi_+(\mathbf{r}) \\ \Psi_-(\mathbf{r}) \end{pmatrix}, \quad (1)$$

where $\Psi_{\pm}(\mathbf{r})$ denotes the envelope wave functions of the corresponding valley states. Here, the valley splitting corresponds to the energy difference between the first excited state and the ground state. The Hamiltonian in Eq. (1) involves

$$H_0(\mathbf{r}) = -\frac{\hbar^2}{2m_t} \left(\frac{\partial^2}{\partial x^2} + \frac{\partial^2}{\partial y^2} \right) - \frac{\hbar^2}{2m_l} \frac{\partial^2}{\partial z^2} + U(\mathbf{r}), \quad (2)$$

where m_l and m_t are the effective mass tensor components at the silicon conduction band minimum and $U(\mathbf{r})$ is the total confinement potential. The intervalley coupling is described by

$$V_c(\mathbf{r}) = \sum_{\mathbf{G}, \mathbf{G}'} c_+^*(\mathbf{G}) c_- (\mathbf{G}') e^{-i(\mathbf{G}-\mathbf{G}'+2\mathbf{k}_0)\cdot\mathbf{r}} U(\mathbf{r}), \quad (3)$$

which involves the plane wave expansion coefficients $c_{\pm}(\mathbf{G}) = c_{\pm\mathbf{k}_0}(\mathbf{G})$ of the lattice-periodic part of the Bloch factors at the two valleys $u_{\pm\mathbf{k}_0}(\mathbf{r}) = \sum_{\mathbf{G}} e^{i\mathbf{G}\cdot\mathbf{r}} c_{\pm\mathbf{k}_0}(\mathbf{G})$. The band index is suppressed throughout this paper, as we are solely concerned with the (lowest-energy) conduction band. A detailed derivation of the coupled envelope equation model (1) can be found in Appendix A.

The total confinement potential

$$U(\mathbf{r}) = U_{\text{het}}(\mathbf{r}) + U_{\text{QD}}(x, y) + U_F(z), \quad (4)$$

describes the effects of both the epitaxial heterostructure and the electrostatic fields induced by the metal gates at the top surface of the device. The heterostructure potential $U_{\text{het}}(\mathbf{r})$ describes the potential induced by the Ge atoms in the SiGe alloy, *i.e.*, a type-II Si/SiGe QW with random alloy disorder, which will be described in more detail in Sec. II B. Note that in the present model, the effects of Ge atoms are entirely described by the heterostructure potential, whereas the underlying band structure (*i.e.*, effective masses and Bloch factors) are those of pure Si. We assume a harmonic QD confinement potential induced by the gate electrodes

$$U_{\text{QD}}(x, y) = \frac{m_t}{2} (\omega_x^2 x^2 + \omega_y^2 y^2), \quad (5)$$

where ω_x and ω_y describe the lateral extension of the QD and thus the orbital splitting $\Delta E_{\text{orb}} = \min(\hbar\omega_x, \hbar\omega_y)$. In the limiting case of $\omega_x = \omega_y$, the QD takes a circular shape. Finally, we assume a constant electric field F along the growth direction, which induces the potential

$$U_F(z) = -e_0 F z, \quad (6)$$

where e_0 is the elementary charge.

B. Heterostructure Potential and Alloy Disorder

The heterostructure potential describes the built-in potential due to the epitaxial profile. In order to account for disorder effects in the $\text{Si}_{1-x}\text{Ge}_x$ alloy, we choose a statistical model similar to that in Refs. [20, 41, 44], where the heterostructure potential is described as a random field

$$U_{\text{het}}(\mathbf{r}) = \Delta E_c \Omega_a \sum_i N_i \delta(\mathbf{r} - \mathbf{R}_i). \quad (7)$$

Here, ΔE_c is the Si/Ge conduction band energy offset [45, 46], $\Omega_a = (a_0/2)^3$ is the atomic volume (not to be confused with the volume of the primitive unit cell) and \mathbf{R}_i is a lattice vector of the (strained) diamond crystal, see Fig. 1 (c)–(e). The number of local Ge atoms at each lattice site is modeled as an independent random variable N_i , which follows a Bernoulli distribution depending on the local Ge concentration $X = X(\mathbf{R}_i)$

$$N_i \sim \text{Bernoulli}(p = X(\mathbf{R}_i)). \quad (8)$$

In the following, we assume a one-dimensional epitaxial profile characterized by $X(\mathbf{r}) = X(z)$ describing the Ge concentration in the QW

$$X(z) = X_b (1 - \Xi(z)), \quad (9)$$

where X_b is the Ge concentration in the barrier (we assume $X_b = 0.3$ throughout) and

$$\Xi(z) = \frac{1}{2} \left(\tanh\left(\frac{h+z}{\sigma_l}\right) + \tanh\left(-\frac{z}{\sigma_u}\right) \right) \quad (10)$$

is a smoothed indicator function that describes the shape of the QW. Here, h is the QW thickness and σ_u and σ_l describe the width of the upper and lower QW interfaces, respectively. The interface widths can be obtained experimentally using scanning transmission electron microscopy, typical values for Si/SiGe QWs are $\sigma_u \approx \sigma_l \approx 0.5$ nm [18, 32, 44].

The heterostructure potential is separated into a deterministic and a random component

$$U_{\text{het}}(\mathbf{r}) = U_{\text{QW}}(z) + \delta U_{\text{het}}(\mathbf{r}), \quad (11)$$

where the deterministic component describes the nominal QW confinement potential given by the expectation value

$$\begin{aligned} U_{\text{QW}}(z) &= \langle U_{\text{het}}(\mathbf{r}) \rangle = \Delta E_c \Omega_a \sum_i X(\mathbf{R}_i) \delta(\mathbf{r} - \mathbf{R}_i) \\ &\approx \Delta E_c X(z). \end{aligned} \quad (12)$$

Here we used the mean value of the Bernoulli-distributed random Ge number at each lattice site $\langle N_i \rangle = X(\mathbf{R}_i)$. The random component has zero mean

$$\langle \delta U_{\text{het}}(\mathbf{r}) \rangle = 0 \quad (13)$$

by construction. Using the covariance of the Bernoulli distribution

$$\langle (N_i - \langle N_i \rangle) (N_j - \langle N_j \rangle) \rangle = \delta_{i,j} X(\mathbf{R}_i) (1 - X(\mathbf{R}_i)),$$

the covariance function of the heterostructure potential is obtained as

$$\begin{aligned} \langle \delta U_{\text{het}}(\mathbf{r}) \delta U_{\text{het}}(\mathbf{r}') \rangle &= \\ &= (\Delta E_c)^2 \Omega_a \delta(\mathbf{r} - \mathbf{r}') \times \\ &\quad \times \Omega_a \sum_i X(\mathbf{R}_i) (1 - X(\mathbf{R}_i)) \delta(\mathbf{r} - \mathbf{R}_i) \\ &\approx (\Delta E_c)^2 \Omega_a X(z) (1 - X(z)) \delta(\mathbf{r} - \mathbf{r}'). \end{aligned} \quad (14)$$

The simple covariance function reflects the assumption of locally independent distribution of Ge atoms stated in Eq. (8) (*i.e.*, no clustering of Ge atoms) and determines the statistical properties of the intervalley-coupling parameter, see Appendix C for details.

C. Empirical Pseudopotential Theory and Strain

The empirical pseudopotential method (EPM) provides an accurate description of the electronic band structure with only a few parameters fitted to experimental data. The approach is particularly efficient for silicon, germanium and other semiconductors [47–49]. A major advantage of the EPM is that it can naturally account for strain effects arising from a displacement of the crystal ions $\mathbf{R}'_i = (I + \varepsilon) \mathbf{R}_i$, where ε is the strain tensor. The key steps for the inclusion of strain in EPM calculations are the consideration of strained reciprocal lattice vectors $\mathbf{G}'_i \approx (I - \varepsilon) \mathbf{G}_i$ (assuming small strain to linear order), the modification of the primitive unit cell volume $\Omega'_p \approx (1 + \text{tr}(\varepsilon)) \Omega_p$, interpolation of the atomic pseudopotentials at the strained lattice vectors and consideration of internal ionic displacement, describing the relative shift between the two sub-lattices, see Fig. 1(e). For strained SiGe alloys, numerous empirical pseudopotential models can be found in the literature [43, 50–55].

In this paper, we use the nonlocal EPM model described by Fischetti & Laux [51]. From this model, we have obtained the plane wave expansion coefficients of the Bloch factors $c_{\mathbf{k}}(\mathbf{G})$, the location of the conduction band minima $\pm \mathbf{k}_0 = (0, 0, \pm k_0)$ and the corresponding effective mass tensor components m_l and m_t by numerical diagonalization of the pseudopotential Hamiltonian (taking 113 plane waves into account). We assume biaxial (tensile) strain due to the lattice mismatch between the $\text{Si}_{0.7}\text{Ge}_{0.3}$ substrate and the Si quantum well [56]

$$\varepsilon_{\text{QW}} = \begin{pmatrix} \varepsilon_{\parallel} & 0 & 0 \\ 0 & \varepsilon_{\parallel} & 0 \\ 0 & 0 & \varepsilon_{\perp} \end{pmatrix} \quad (15)$$

with $\varepsilon_{\parallel} = \varepsilon_{x,x} = \varepsilon_{y,y} = a_0^{\text{SiGe}}/a_0^{\text{Si}} - 1 \approx 1.14\%$ and $\varepsilon_{\perp} = \varepsilon_{z,z} = -2C_{12}/C_{11}\varepsilon_{\parallel} \approx -0.88\%$, where $C_{1,2}$ and $C_{2,2}$ are elastic constants of Si [51]. Below, we will consider additional shear strain, which might originate from the macroscopic device geometry [33, 57, 58], dislocations [59, 60] or alloy disorder [61–63].

D. Perturbation Theory

The valley splitting can be approximated by first-order degenerate perturbation theory [15] assuming that both the intervalley-coupling potential $V_c(\mathbf{r})$ and the alloy-disorder potential $\delta U_{\text{het}}(\mathbf{r})$ are small. In this case, the problem (1) is to zeroth order approximated by

$$\left(-\frac{\hbar^2}{2} \nabla \cdot (m^{-1} \nabla) + \langle U(\mathbf{r}) \rangle \right) \Psi_0(\mathbf{r}) = E_0 \Psi_0(\mathbf{r}),$$

where $\langle U(\mathbf{r}) \rangle = U_{\text{QD}}(x, y) + U_{\text{QW}}(z) + U_F(z)$ is the mean potential energy. The reduced zeroth-order problem describes two energetically degenerate valley states with identical orbital wave function $\Psi_0(\mathbf{r})$. Using the separation ansatz $\Psi_0(\mathbf{r}) = \phi_0(x, y) \psi_0(z)$ and $E_0 = E_{t,0} + E_{l,0}$,

the problem decouples into two scalar effective mass-type Schrödinger equations, *i.e.*, the transverse problem

$$\left(-\frac{\hbar^2}{2m_t} \left(\frac{\partial^2}{\partial x^2} + \frac{\partial^2}{\partial y^2} \right) + U_{\text{QD}}(x, y) \right) \phi_n(x, y) = E_{t,n} \phi_n(x, y) \quad (16)$$

and the longitudinal problem

$$\left(-\frac{\hbar^2}{2m_l} \frac{\partial^2}{\partial z^2} + U_{\text{QW}}(z) + U_F(z) \right) \psi_n(z) = E_{l,n} \psi_n(z). \quad (17)$$

The exact ground state wave function of the transverse problem reads

$$\phi_0(x, y) = (\pi l_x l_y)^{-1/2} e^{-\frac{1}{2} \left(\frac{x}{l_x} \right)^2} e^{-\frac{1}{2} \left(\frac{y}{l_y} \right)^2} \quad (18)$$

with ground state energy $E_{t,0} = (\hbar\omega_x + \hbar\omega_y)/2$ and QD width $l_j = \sqrt{\hbar/(m_t\omega_j)}$, $j \in \{x, y\}$. The ground state $\{E_{l,0}, \psi_0(z)\}$ of the longitudinal problem is obtained numerically using a finite difference approximation.

In first-order perturbation theory, the multi-valley envelope function in Eq. (1) for the degenerate ground state subspace is taken as $(\Psi_+(\mathbf{r}), \Psi_-(\mathbf{r}))^T \approx (\eta_+, \eta_-)^T \Psi_0(\mathbf{r})$, which after integration with $\Psi_0^*(\mathbf{r})$ yields the reduced problem

$$\begin{pmatrix} E_0 + \delta E_0 & \Delta \\ \Delta^* & E_0 + \delta E_0 \end{pmatrix} \begin{pmatrix} \eta_+ \\ \eta_- \end{pmatrix} = E \begin{pmatrix} \eta_+ \\ \eta_- \end{pmatrix}. \quad (19)$$

Here, $\delta E_0 = \int d^3r \delta U_{\text{het}}(\mathbf{r}) \Psi_0^2(\mathbf{r})$ is a random shift of the energy level (that has no further physical implications) and the parameter

$$\begin{aligned} \Delta &= \int d^3r \Psi_0^*(\mathbf{r}) V_c(\mathbf{r}) \Psi_0(\mathbf{r}) \\ &= \sum_{\mathbf{G}, \mathbf{G}'} c_+^*(\mathbf{G}) c_- (\mathbf{G}') \times \\ &\quad \times \int d^3r e^{-i(\mathbf{G}-\mathbf{G}'+2\mathbf{k}_0) \cdot \mathbf{r}} U(\mathbf{r}) \Psi_0^2(\mathbf{r}) \end{aligned} \quad (20)$$

is the complex-valued intervalley-coupling strength. We note that Eq. (20) involves all of the aforementioned effects, *i.e.*, strain (via modification of the reciprocal lattice vectors and the Bloch factor expansion coefficients), alloy disorder and non-trivial resonances due to coupling of valley states within different Brillouin zones. Finally, the energy splitting of the two valley states described by the reduced problem (19) is obtained as

$$E_{\text{VS}} = 2|\Delta|. \quad (21)$$

A comprehensive theoretical description of the intervalley-coupling parameter provides the key to the engineering of deterministic enhancements of the valley splitting in Si/SiGe qubits.

E. Intervalley Coupling Parameter

The intervalley coupling parameter Δ given in Eq. (20) has a deterministic and a random component

$$\Delta = \Delta_{\text{det}} + \Delta_{\text{rand}}, \quad (22)$$

reflecting the deterministic and stochastic components of the total confinement potential (4). In the following, we will evaluate both components.

1. Deterministic Component

The deterministic component

$$\Delta_{\text{det}} = \Delta_{\text{det}}^l + \Delta_{\text{det}}^t \quad (23)$$

comprises a transverse and a longitudinal contribution corresponding to the confinement potentials of the two decoupled effective mass equations (16)–(17). Using the exact ground state wave function (18) of the transverse problem, the in-plane integration can be evaluated explicitly. With this, one arrives at

$$\begin{aligned} \Delta_{\text{det}}^l &= \sum_{\mathbf{G}, \mathbf{G}'} c_+^*(\mathbf{G}) c_- (\mathbf{G}') \times \\ &\times e^{-\frac{1}{4}(G_x - G'_x)^2 l_x^2} e^{-\frac{1}{4}(G_y - G'_y)^2 l_y^2} \times \\ &\times \int dz e^{-i(G_z - G'_z + 2k_0)z} (U_{\text{QW}}(z) + U_F(z)) \psi_0^2(z) \end{aligned} \quad (24)$$

and

$$\begin{aligned} \Delta_{\text{det}}^t &= \sum_{\mathbf{G}, \mathbf{G}'} c_+^*(\mathbf{G}) c_- (\mathbf{G}') \times \\ &\times e^{-\frac{1}{4}(G_x - G'_x)^2 l_x^2} e^{-\frac{1}{4}(G_y - G'_y)^2 l_y^2} \times \\ &\times \left[\frac{\hbar \omega_x}{2} \left(\frac{1}{2} - \frac{(G_x - G'_x)^2 l_x^2}{4} \right) \right. \\ &\quad \left. + \frac{\hbar \omega_y}{2} \left(\frac{1}{2} - \frac{(G_y - G'_y)^2 l_y^2}{4} \right) \right] \times \\ &\times \int dz e^{-i(G_z - G'_z + 2k_0)z} \psi_0^2(z). \end{aligned} \quad (25)$$

Deterministic enhancements of the valley splitting can be achieved, when the product of the confinement potential and the longitudinal wave function component resonate with the complex exponential in Eq. (24), cf. Ref. [31]. This means, that the Fourier spectrum of

$$S(z) = (U_{\text{QW}}(z) + U_F(z)) \psi_0^2(z)$$

must provide large amplitudes $\tilde{S}(q)$ at wave numbers q that obey the resonance condition

$$G_z - G'_z + 2k_0 - q = 0 \quad (26)$$

for any possible combination of G_z and G'_z . In this case,

$$\int dz e^{-i(G_z - G'_z + 2k_0)z} S(z) = 2\pi \tilde{S}(G_z - G'_z + 2k_0)$$

gives a strong contribution via an enhancement of the coupling strength between certain valley states, possibly across different Brillouin zones. A similar reasoning holds true for an enhancement of the transverse component (25) with correspondingly adapted $S(z)$, but for typical parameter values the longitudinal component (24) is dominant. This concept of confinement potential engineering to achieve large Fourier amplitudes $\tilde{S}(q)$ is explicitly addressed in the wiggly well proposal [31, 33, 34], but is implicitly exploited also in other approaches (*e.g.*, sharp interfaces [24], Ge-spike [35]).

The two expressions (24) and (25) can be considerably simplified by exploiting the fact that the in-plane extension of the QD wave function is much larger than the lattice constant $l_x, l_y \gg a_0$. With this, the Gaussians (second line of both expressions), effectively reduce to a Kronecker-Delta reproducing the selection rule for quantum wells [16]. In the limit of small strain, this approximation, which is described in detail in Appendix B, allows for a very compact notation

$$\Delta_{\text{det}} = \sum_{n=-\infty}^{\infty} \Delta_{\text{det},n} = \sum_{n=-\infty}^{\infty} C_n^{(2)} J_n^{\text{det}}, \quad (27)$$

where we have introduced the effective band structure coefficients $C_n^{(2)}$ described in Eq. (B3) and the integrals J_n^{det} defined in Eq. (B10). The compact form allows for a fast numerical evaluation, where a single summation over a few integers replaces the tedious double summation over the reciprocal lattice vectors in Eqs. (24)–(25).

The above expressions fully account for strain (to linear order) and non-trivial resonances due to coupling with valley states in neighboring Brillouin zones. Hence, the present model goes beyond the commonly employed “ $2k_0$ -theory”, which accounts only for the $n = 0$ contribution in Eq. (27). This corresponds to the trivial resonance condition $\mathbf{G} = \mathbf{G}'$, cf. Ref. [16], where only the spectral component at

$$q|_{n=0} = 2k_0 \quad (28)$$

is taken into account. The plot of the band structure coefficients in Fig. 2 (a) shows, that this approximation is indeed justified in many scenarios, but might fail when the integrands of Eqs. (24)–(25) exhibit strong non-trivial resonances, *i.e.*, with $\mathbf{G} - \mathbf{G}' = n\mathbf{G}_0$ for $n \neq 0$ and \mathbf{G}_0 given in Eq. (B4). In these cases, contributions proportional to band structure coefficients $C_{n \neq 0}^{(2)}$ become relevant. A particularly important resonance is the one mediated by $C_{n=-1}^{(2)}$ at

$$q|_{n=-1} = -2k_1, \quad (29)$$

that is associated with the long-period wiggly-well [31, 33, 34]. Here we introduced

$$k_1 = \frac{2\pi}{a_0} (1 - \varepsilon_{z,z}) - k_0, \quad (30)$$

which is the reciprocal-space distance of the valley states from the Brillouin zone boundary, see Fig. 1 (a). We note

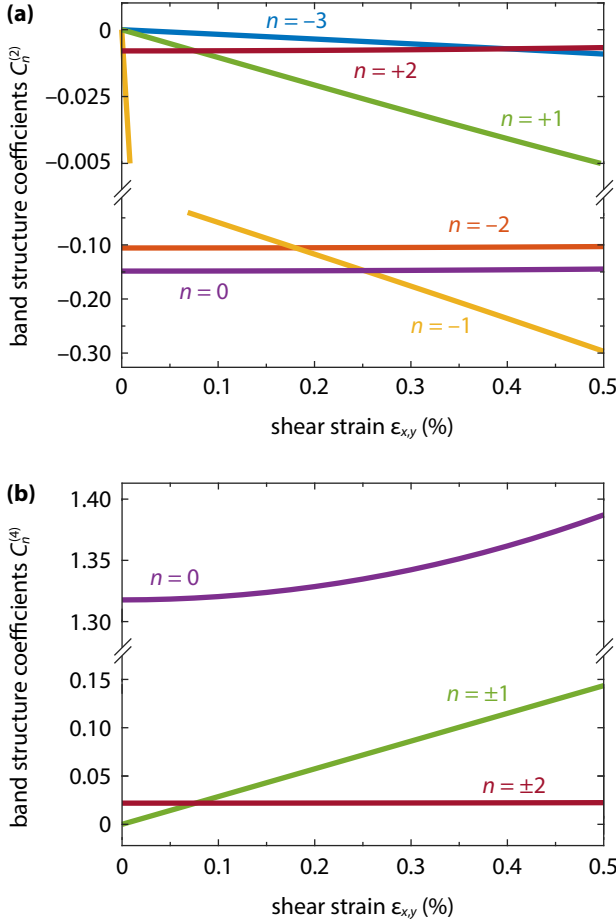


Fig. 2. (a) Band structure coefficients $C_n^{(2)}$ governing the magnitude of the deterministic contribution to the valley splitting as a function of shear strain $\varepsilon_{x,y}$. The coefficients have been computed from Eq. (B3) using plane wave expansions of the Bloch factors for strained silicon at the conduction band minimum. In addition to shear strain, biaxial tensile strain arising from the Si/Si_{0.7}Ge_{0.3} heterostructure was assumed, see Eq. (15). Coefficients with odd n show a linear dependence on shear strain, while coefficients with even n are practically constant. (b) Same as (a) for the band structure coefficients $C_n^{(4)}$ given by Eq. (B9) governing the magnitude of the disorder-induced contribution to the valley splitting.

that uniaxial strain $\varepsilon_{z,z}$ (which is typically compressive) leads to a slight modification of this distance. As shown in Fig. 2, the band structure coefficient $C_{n=-1}^{(2)}$ obtained from the EPM is linearly dependent on the shear strain component as $C_{n=-1}^{(2)} \approx -0.589 \times \varepsilon_{x,y}$. This result is in good agreement with the theory recently presented by Woods *et al.* [33], which predicts a linear dependency of the long-period wiggles on shear strain following a $sp^3d^5s^*$ tight-binding model. One can clearly see that the resonance is suppressed in the absence of shear strain $\varepsilon_{x,y} = 0$, which is explained by a nonsymmorphic screw symmetry of the (either relaxed or biaxially strained) silicon crystal structure [31, 33]. In the presence of shear

strain, however, this symmetry is broken such that the resonance at $n = -1$ yields enhancements also for other strategies much simpler than the long-period wiggles, *e.g.*, sharp interfaces or uniform Ge concentrations in the QW. This is discussed in more detail along with numerical results in Sec. III below. Finally, in Sec. III we also observe small contributions from the non-trivial $n = -2$ resonance, in particular at sharp interfaces. This corresponds to

$$q|_{n=-2} = -2k_0 - 4k_1 \quad (31)$$

i.e., a coupling between distant valley states separated by an intermediate Brillouin zone. The impact of further non-trivial resonances was found to be negligible.

2. Random Component

The random contribution to the valley splitting in Eq. (22) results from alloy disorder and is described by

$$\Delta_{\text{rand}} = \sum_{\mathbf{G}, \mathbf{G}'} c_+^*(\mathbf{G}) c_- (\mathbf{G}') \times \int d^3r e^{-i(\mathbf{G}-\mathbf{G}'+2\mathbf{k}_0)\cdot\mathbf{r}} \delta U_{\text{het}}(\mathbf{r}) \Psi_0^2(\mathbf{r}). \quad (32)$$

As shown in Appendix C1, Δ_{rand} obeys a complex normal distribution

$$\Delta_{\text{rand}} \sim \text{ComplexNormal}(\mu = 0, \Gamma, C), \quad (33)$$

with zero mean $\mu = 0$, covariance $\Gamma = \langle |\Delta_{\text{rand}}|^2 \rangle$ and relation (or pseudo-covariance) parameter $C = \langle \Delta_{\text{rand}}^2 \rangle$. As the relation parameter is typically negligible in comparison to the covariance, the random contribution is well approximated by a circular symmetric normal distribution in the complex plane with independent and identically distributed real and imaginary parts

$$\begin{aligned} \text{Re}(\Delta_{\text{rand}}) &\sim \text{Normal}\left(\mu = 0, \sigma^2 = \frac{1}{2} \langle |\Delta_{\text{rand}}|^2 \rangle\right), \\ \text{Im}(\Delta_{\text{rand}}) &\sim \text{Normal}\left(\mu = 0, \sigma^2 = \frac{1}{2} \langle |\Delta_{\text{rand}}|^2 \rangle\right). \end{aligned}$$

We refer to Appendix C1 for a detailed derivation. Consequently, the characterization of the disorder-induced component to the valley splitting requires solely the computation of the covariance $\langle |\Delta_{\text{rand}}|^2 \rangle$. Using the covariance function of the random potential (14) and the in-plane wave functions (18), one obtains

$$\begin{aligned} \langle |\Delta_{\text{rand}}|^2 \rangle &= \frac{1}{2\pi l_x l_y} (\Delta E_c)^2 \Omega_a \times \\ &\times \sum_{\mathbf{G}, \mathbf{G}'} \sum_{\mathbf{K}, \mathbf{K}'} c_+^*(\mathbf{G}) c_- (\mathbf{G}') c_+ (\mathbf{K}) c_- (\mathbf{K}') \times \\ &\times e^{-\frac{1}{2} \left(\frac{(G_x - G'_x - K_x + K'_x)l_x}{2} \right)^2} e^{-\frac{1}{2} \left(\frac{(G_y - G'_y - K_y + K'_y)l_y}{2} \right)^2} \times \\ &\times \int dz e^{-i(G_z - G'_z - K_z + K'_z)z} X(z) (1 - X(z)) \psi_0^4(z). \end{aligned} \quad (34)$$

Following the same steps as in the deterministic part above, the fourfold summation over reciprocal lattice vectors can be reduced to a single summation

$$\langle |\Delta_{\text{rand}}|^2 \rangle = \sum_{n=-\infty}^{\infty} C_n^{(4)} J_n^{\text{rand}}, \quad (35)$$

where the integrals J_n^{rand} are given in Eq. (B8) and the band structure coefficients $C_n^{(4)}$ are defined in Eq. (B9). We refer to Appendix B for details. The band structure coefficients $C_n^{(4)}$ are shown as a function of shear strain in Fig. 2 (b). In contrast to the deterministic part, non-trivial resonances are less pronounced in the disorder-induced contribution to the valley splitting such that Eq. (35) is in fact largely dominated by the trivial contribution proportional to $C_{n=0}^{(4)}$. In general, modifications due to shear strain are weaker for the random component than for the deterministic part.

3. Valley Splitting Statistics

From the normal distribution of Δ_{rand} it follows that the valley splitting obeys a Rice distribution

$$E_{\text{VS}} \sim \text{Rice} \left(\nu = 2 |\Delta_{\text{det}}|, \sigma^2 = 2 \langle |\Delta_{\text{rand}}|^2 \rangle \right), \quad (36)$$

see Appendix C 2 for details. This result has been obtained previously using the $2k_0$ -theory in Refs. [18, 19] with a very similar model for the alloy disorder. Here, it has been extended to a more complex case that includes non-trivial resonances and strain. We find that the qualitative result of a Rice distribution for E_{VS} is unchanged under these extensions, but the shape parameters of the distribution $\nu = 2 |\Delta_{\text{det}}|$ and $\sigma^2 = 2 \langle |\Delta_{\text{rand}}|^2 \rangle$ are modified to account for the more complex physics, see Eqs. (24)–(25) and (34).

The Rice distribution was found to be in good agreement with fully atomistic tight-binding simulations [18, 32], density functional theory [44] and experimental results from conveyor-mode shuttling tomography of the valley splitting [30].

In the following, we will frequently consider the mean and variance of the Rice distribution given by

$$\langle E_{\text{VS}} \rangle = \sqrt{\frac{\pi}{2}} \sigma f \left(\left(\frac{\nu}{2\sigma} \right)^2 \right) \quad (37)$$

$$\text{Var} (E_{\text{VS}}) = 2\sigma^2 + \nu^2 - \langle E_{\text{VS}} \rangle^2 \quad (38)$$

with the shape parameters ν and σ specified above. The expression for the mean involves the (monotonically increasing) function

$$f(x) = e^{-x} ((1 + 2x) I_0(x) + 2x I_1(x)),$$

where $I_n(x)$ denotes the modified Bessel functions of first kind. The asymptotics

$$f(x) \sim \begin{cases} 1 + x & x \ll 1 \\ 2\sqrt{2x/\pi} & x \gg 1 \end{cases}$$

symbol	description	value
ΔE_c	Si/Ge conduction band offset	0.5 eV
X_b	mean barrier Ge concentration	0.3
$\hbar\omega_x, \hbar\omega_y$	orbital splitting energy (circular QD)	3.0 meV
F	electric field strength	5 mV/nm
σ_u, σ_l	upper and lower QW interface width	0.5 nm
h	quantum well thickness	75 ML

Tab. I. Parameter values used in the computations, if not stated otherwise. Band structure parameters (including effective masses) were computed as a function of strain using the empirical pseudopotential model described in Ref. [51] with parameters stated there. The QW thickness is given in units of monolayers ML = $a_0/4$ of the relaxed Si crystal.

indicate that the expected valley splitting is dominated by the deterministic part only if $\nu \gg 2\sigma$, but is disorder-dominated otherwise:

$$\langle E_{\text{VS}} \rangle \sim \begin{cases} \sqrt{\frac{\pi}{2}} \sigma & \nu \ll 2\sigma, \\ \nu & \nu \gg 2\sigma. \end{cases}$$

In order to distinguish between regimes with primarily deterministic or disorder-dominated contributions to the mean valley splitting, we consider the separatrix defined by the condition

$$\left. \frac{\nu}{\langle E_{\text{VS}} \rangle} \right|_{\text{separatrix}} = \frac{1}{2}, \quad (39)$$

where both components contribute with equal weight. The separatrix condition can be solved explicitly for the shape parameters as

$$\left. \frac{\nu}{2\sigma} \right|_{\text{separatrix}} \approx 0.3507$$

where $x_0 \approx 0.3507$ satisfies $f(x_0^2) = 4\sqrt{2/\pi} x_0$, which reflects Eq. (39).

III. RESULTS

In this section, the model described in Sec. II is employed to compute the valley splitting for different types of engineered heterostructures. We will specifically highlight the effects of shear strain and non-trivial resonances, that go beyond previously reported results. Parameter values used in the computations are given in Tab. I.

A. Conventional Heterostructure: Dependence on Quantum Well Interface Width

Sharp interfaces are a common strategy to enhance the valley splitting [16, 24, 64]. From the perturbative expression for the intervalley coupling parameter in Eq. (20), it is clear that any heterostructure which contains sufficiently sharp spatial features overlapping with the wave

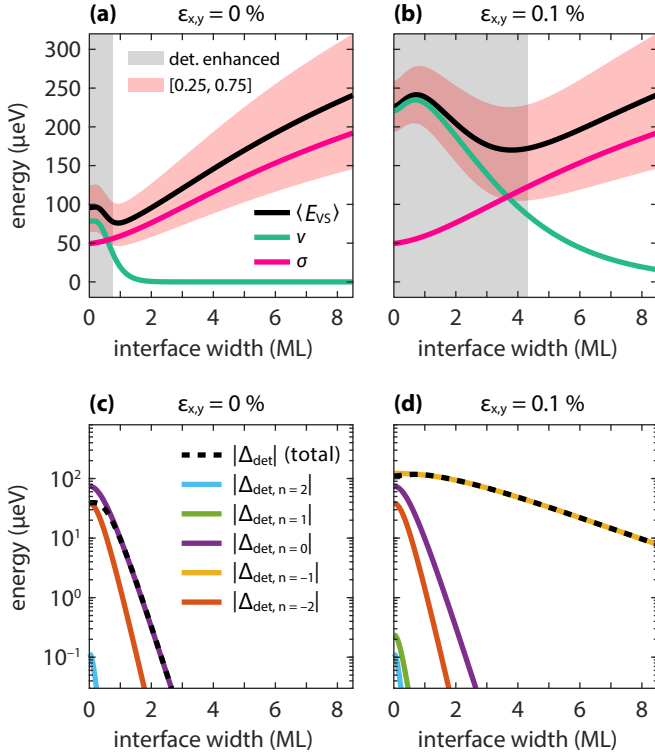


Fig. 3. Impact of interface width on valley splitting. (a) Mean valley splitting $\langle E_{VS} \rangle$ and shape parameters ν and σ of the Rice distribution in the absence of shear strain $\epsilon_{x,y} = 0$ as a function of the QW interface width, cf. Eq. (10). The interface width is given in units of monolayers $\text{ML} = a_0/4 \approx 0.1357$ nm of relaxed Si. The gray shaded region indicates the deterministically enhanced regime according to Eq. (39) and the red shaded region shows the [25%, 75%] quantile of the Rice distribution. Deterministic enhancements are observed for sharp interfaces with up to one ML width. (b) Same as (a), but for small shear strain $\epsilon_{x,y} = 0.1\%$. The deterministically enhanced regime is extended to about four MLs. (c) Absolute values of the individual components $\Delta_{det,n}$ contributing to the deterministic valley splitting, see Eq. (27), as a function of the interface width. In the absence of shear strain, the resulting valley splitting is dominated by the $n = 0$ and $n = -2$ resonances in the deterministically enhanced regime, whereas the $n = 0$ resonance dominates in the disorder-dominated regime. (d) In the case of small shear strain $\epsilon_{x,y} = 0.1\%$ the $n = -1$ component is the dominant contribution over the entire parameter domain. In the simulation, an electric field of $F = 10$ mV/nm was assumed.

function will lead to an enhanced valley splitting. This is because the corresponding broadband Fourier spectrum still has comparatively large amplitudes even at high wave numbers, especially close to $2k_0$. Consequently, there is a great potential for further enhancement of the valley splitting in the presence of shear strain $\epsilon_{x,y} \neq 0$, which unlocks the low-frequency resonance at $2k_1$ that is typically supported by much larger Fourier amplitudes.

The results in Fig. 3 show indeed, that the influence of shear strain on sharp interfaces can be significant. Without shear strain, extremely sharp interfaces with a

width $\sigma_{u,l} \lesssim a_0/4$ of less than one monolayer (ML) are required to achieve a deterministic enhancement of the valley splitting, see Fig. 3(a). This result is consistent with previous findings based on the $2k_0$ -theory [19, 20]. If shear strain is applied, the range in which a deterministic enhancement can be expected is considerably increased. In Fig. 3(b) it is shown that already moderate shear strain of $\epsilon_{x,y} = 0.1\%$ yields deterministic enhancements for rather broad interfaces with a width of up to four MLs. Correspondingly, the valley splitting is increased approximately by a factor of two. In any case, sharp interfaces should be combined with a strong electric field across the QW, in order to enhance the weight of the high-frequency Fourier components by a large overlap of the wave function with the interface.

B. Unconventional Heterostructures

A very promising approach to achieve deterministic enhancements of the valley splitting is the *wiggle well* heterostructure, which employs an oscillating Ge concentration within the QW [31, 33, 34]. In the following, we assume an epitaxial profile of the form

$$X(z) = X_{\text{QW}}(z) + \Xi(z)x(z),$$

where $X_{\text{QW}} = X_b(1 - \Xi(z))$ is the profile of the conventional SiGe/Si/SiGe QW, see Eq. (9), and

$$x(z) = \frac{X_{\text{ww}}}{2}(1 + \cos(qz)), \quad (40)$$

describes the oscillating Ge concentration in the QW with amplitude X_{ww} and wave number q . The smoothed QW indicator function $\Xi(z)$ is given in Eq. (10).

In the following, we will discuss a number of special cases of Eq. (40) that are each characterized by a particular wave number q .

1. Uniform Germanium Concentration

For $q = 0$, the profile in Eq. (40), reduces to a uniform Ge concentration in the QW. In this configuration, which was first proposed in Ref. [18], the mean valley splitting is enhanced because the random Ge concentration corresponds to a flat (white noise) power spectrum in reciprocal space, contributing even at large wave numbers. The corresponding of the valley splitting enhancement is, however, entirely disorder-dominated. Therefore, numerous spin-valley hotspots must be expected [27].

For a sufficient amount of shear strain, when the deterministic component starts to be dominated by the $n = -1$ resonance, cf. Fig. 3(d), slight enhancements of the deterministic contribution can be expected. These enhancements are, however, much smaller than the disorder-induced component for typical parameters. This is shown in Fig. 4(a)–(b), where the valley splittings at $q = 0$

are practically unchanged even in the presence of shear strain. Moreover, Fig. 5(b) shows a regime with enhanced mean valley splitting at very low wave numbers, which is clearly outside of the deterministically enhanced regime (indicated by the separatrix condition (39), dashed line). Finally, the typical epitaxial profile and electron density distribution is shown in Fig. 5(c) along with the power spectral density (PSD) of the product $(U_{QW}(z) + U_F(z))\psi_0^2(z)$ and the complex-plane distribution of the intervalley coupling parameter Δ , showing that the valley splitting is indeed disorder-dominated.

2. Short-Period Wiggle-Well

The results shown in Fig. 4 feature a strong resonance at $q = 2k_0$, which grows with increasing Ge amplitude X_{ww} , but is practically independent of shear strain. This configuration is called the *short-period wiggle-well*. The effect is based on a direct enhancement of the coupling between the valley states within the same Brillouin zone triggered by the periodicity of the confinement potential. The short-period wiggle-well requires a high-frequency Ge modulation with a very short wave length $\lambda = \pi/k_0 \approx 2.4 \text{ ML} \approx 0.32 \text{ nm}$. The epitaxial growth of such rapidly modulated structures is out of reach with current technology, which is why the short-period wiggle-well is not relevant for practical applications.

3. Long-Period Wiggle-Well

In the presence of shear strain, a second resonance emerges at $q = 2k_1$, see Fig. 4(b), where k_1 has been defined in Eq. (30). This resonance is associated with the so-called *long-period wiggle-well* [31, 33, 34], which enhances the coupling of valley states in neighboring Brillouin zones separated by $2k_1$. The corresponding wave length is $\lambda \approx 12.4 \text{ ML} \approx 1.68 \text{ nm}$. Epitaxial growth of such structures is feasible using molecular beam epitaxy.

The dependency on shear strain is illustrated in Fig. 4(c), showing a linear relation between the mean valley splitting and shear strain. In addition, the plot shows that the standard deviation of the valley splitting (dashed lines) is much smaller than the mean value. This indicates a strong deterministic enhancement of the valley splitting achieved by the long-period wiggle well.

The two-parametric plot in Fig. 5(a) shows the dependency of the mean valley splitting in a long-period wiggle-well on shear strain and the Ge amplitude. The separatrix (dashed line) indicates that a minimum shear strain of about $\varepsilon_{x,y} \approx 0.02\%$ is required to enter the deterministically enhanced regime even for high Ge amplitudes. For larger shear strains above $\varepsilon_{x,y} \gtrsim 0.08\%$, however, the deterministic enhancement sets in already for tiny Ge amplitudes (but then also with very small mean valley splittings). In Fig. 5(b), the mean valley splitting $\langle E_{VS} \rangle$

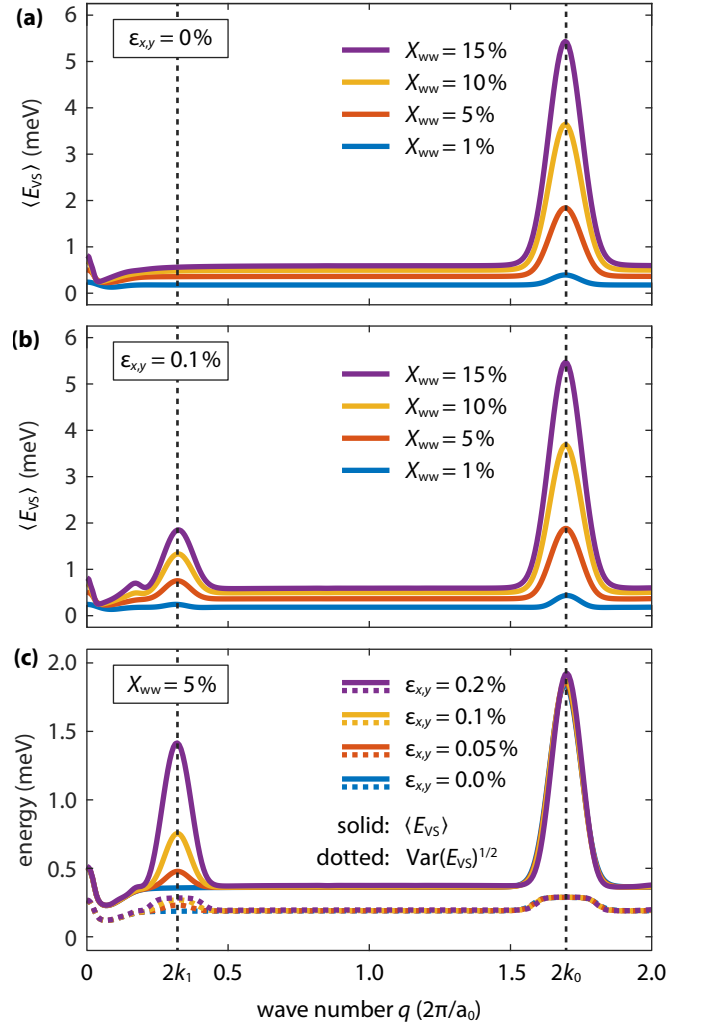


Fig. 4. Mean valley splitting in the wiggle well heterostructure as a function of wave number. (a) In the absence of shear strain $\varepsilon_{x,y} = 0\%$ deterministic enhancements are observed only at $q = 2k_0$ (short-period wiggle-well), which increases with increasing amplitude X_{ww} . Away from the resonance, the non-zero valley splittings are disorder-dominated. (b) A small amount of shear strain $\varepsilon_{x,y} = 0.1\%$ unlocks a new resonance at $q = 2k_1$ (long-period wiggle-well). (c) Mean (solid lines) and standard deviation (dashed line) of the valley splitting for fixed amplitude $X_{ww} = 5\%$ and different values of shear strain $\varepsilon_{x,y}$. A constant electric field $F = 5 \text{ mV/nm}$ and biaxial tensile strain, see Eq. (15), was assumed in the simulations.

is shown for fixed shear strain $\varepsilon_{x,y} = 0.07\%$ as a function of the wave number q and the Ge oscillation amplitude X_{ww} . The broad resonance around $q \approx 2k_1$ falls clearly in the deterministically enhanced regime and is relatively robust against deviations from the ideal wave number. The typical epitaxial profile and the corresponding electron density distribution are shown in Fig. 5(e) along with the PSD and the complex-plane distribution of the intervalley coupling parameter (inset). The strong spectral contribution at $2k_1$ leads to a strong deterministic enhancement of the valley splitting such that the complex normal distribution

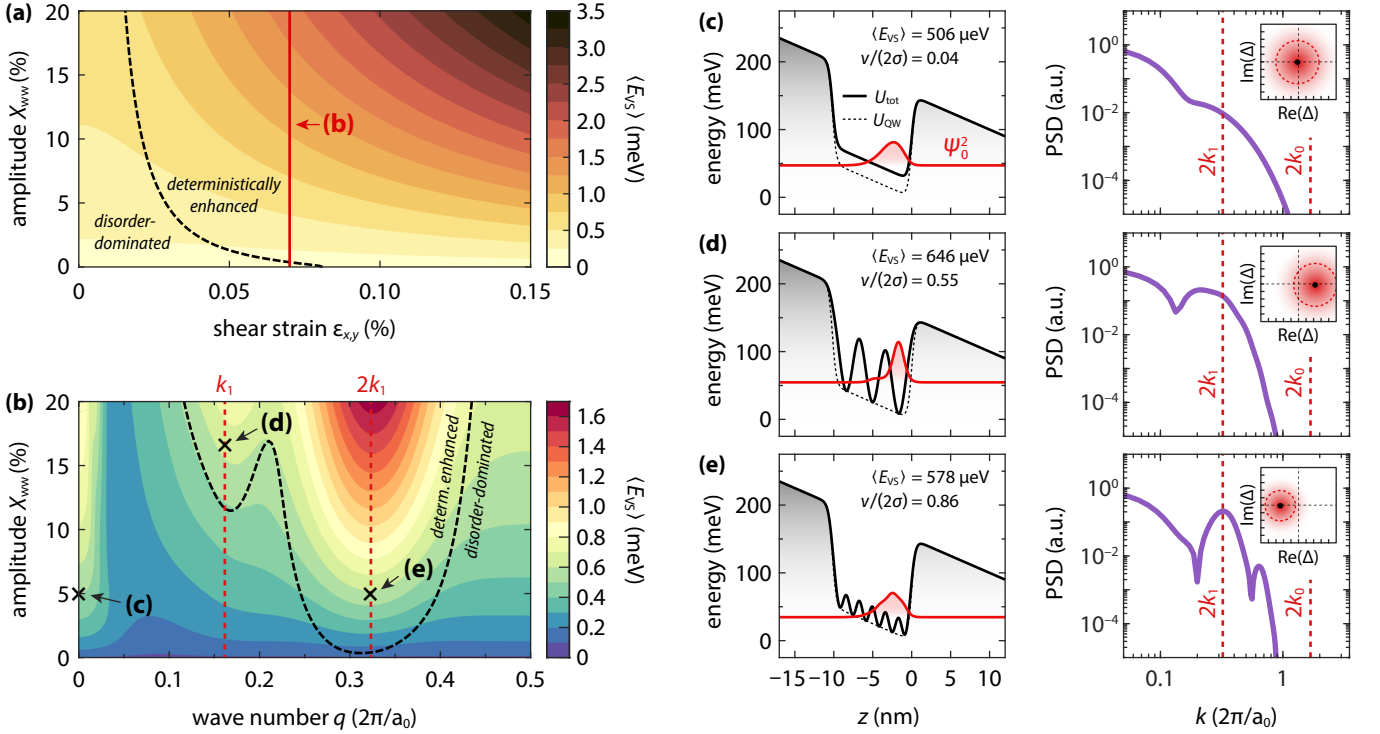


Fig. 5. (a) Mean valley splitting of the long-period wigggle-well with fixed wave number $q = 0.32 \times 2\pi/a_0 \approx 2k_1$ as a function of shear strain $\varepsilon_{x,y}$ and Ge amplitude X_{ww} . The dashed line is the separatrix defined in Eq. (39) that separates disorder-dominated and deterministically enhanced regimes. For large shear strains, a deterministic enhancement is achieved already for very small Ge amplitudes. The red line indicates the constant shear strain value considered in panel (b). (b) Mean valley splitting as a function of wave number q and amplitude X_{ww} for fixed shear strain $\varepsilon_{x,y} = 0.07\%$. Three domains with valley splitting enhancements can be observed, namely, at very low $q \approx 0$ (nearly constant uniform Ge concentration in the QW), near $q \approx k_1$ (lower harmonic/ Ge spike, only for sufficiently high X_{ww}) and near $q \approx 2k_1$ (long-period wigggle-well). The dashed line is again the separatrix. (c) Left: Epitaxial profile and ground state electron density distribution for the uniform Ge concentration in the well ($q = 0$, $X_{ww} = 0.05$) at shear strain $\varepsilon_{x,y} = 0.07\%$. The ratio $\nu/(2\sigma)$ indicates that this configuration falls into the disorder-dominated regime. Right: Power spectral density (PSD) of the product $(U_{QW}(z) + U_F(z))\psi_0^2(z)$ as a function of the wave number k . The contribution to the valley splitting is dominated by the $2k_1$ -resonance and is thus larger than predicted by the $2k_0$ -theory. The inset shows the statistical distribution of the intervalley coupling parameter in the complex plane in the range of $-0.5 \text{ meV} \leq \text{Re}(\Delta), \text{Im}(\Delta) \leq 0.5 \text{ meV}$. (d) Same as (c), but at ($q = k_1$, $X_{ww} = 0.17$). The product of the potential and the wave function yields a strong Fourier component at $k = 2k_1$, despite the potential having only half of the frequency $q = k_1$. The configuration has a moderate deterministic enhancement $\nu/(2\sigma) \approx 0.55$. (e) Same as (c), but for a long-period wigggle-well at ($q = 2k_1$, $X_{ww} = 0.05$). The $q = 2k_1$ -periodic modulation of the potential provides a significant deterministic enhancement of the valley splitting $\nu/(2\sigma) \approx 0.86$. A constant electric field $F = 5 \text{ mV/nm}$ and biaxial (tensile) strain was assumed in all simulations.

governing the statistical properties is steered away from the origin. Hence, a significant suppression of spin-valley hotspots can be expected. The long-period wigggle-well is therefore a very promising approach to design qubits with deterministically large valley splittings.

4. Lower Harmonic Wigggle-Well / Ge-Spike

Finally, we note the emergence of a new resonance in Fig. 4(b) at approximately $q \approx k_1$, i.e., about half the wave number of the long-period wigggle-well. This lower harmonic resonance is suppressed in the absence of shear strain and sets in only at fairly high Ge amplitudes. The resonance is also clearly visible in Fig. 5(b) for Ge am-

plitudes above $X_{ww} \geq 12\%$ and falls clearly within the deterministically enhanced regime. The underlying mechanism becomes clear in Fig. 5(d), which shows an intricate interplay of the periodic heterostructure potential and the electron ground state wave function. While both of them individually have a frequency spectrum dominated by the k_1 -component, their combination effectively triggers the $2k_1$ -resonance mechanism that underlies the long-period wigggle-well. From the plot it becomes also clear why a large Ge amplitude is required, since this is crucial to achieve the strong confinement of the electron wave function.

While at first glance the longer wave length might be favorable due to reduced demands on the epitaxial growth process, the required high Ge content causes severe

drawbacks. In fact, we expect a strong enhancement of the spin-orbit interaction in such a structure [65], which would significantly complicate the control of the qubit. The deterministic enhancements achieved with such a structure are lower than that of a corresponding long-period wiggles-well.

Finally, we remark that the second Ge-peak near the lower interface is not essential for the observed effect. It is simply enforced by the parametrization in Eq. (40). Without the second Ge-peak, the structure has strong similarities with the Ge-spike described in Ref. [35].

IV. DISCUSSION

The theoretical model developed in Sec. II of this work combines a number of previously existing modeling concepts into a unified framework. In this way, a comprehensive description of a number of important effects contributing to the valley splitting in engineered heterostructures, *i.e.*, alloy-disorder, strain and resonances, has been achieved at the level of envelope function theory.

The numerical results in Sec. III are consistent with previously reported findings, but also extend them in view of a systematic investigation of strain effects. For instance, significant shear strain-induced enhancements of the valley splitting even at wide interfaces were predicted. In addition, the model includes all non-trivial resonances that mediate intervalley coupling across neighboring Brillouin zones. Most notably, this includes the important resonance at $2k_1$, which triggers the mechanism behind the long-period wiggles-well. This is the main difference with the prevailing $2k_0$ -theory, which does not explain the long-period wiggles-well. The key accomplishments of the $2k_0$ -theory as described in Refs. [19, 20], lies in the description of disorder-induced effects and the distinction between deterministic and disorder-dominated enhancements of valley splitting. This part of the theory has been adopted practically identically in the present model.

The model presented in this paper differs in a number of aspects from the model by Feng & Joynt [31], which has been the first to provide an explanation for the mechanism behind the long-period wiggles-well in the framework of envelope function theory. The mechanism proposed there to induce a violation of the nonsymmorphic screw symmetry – which otherwise suppresses the resonance at $2k_1$ – is based on a randomization of the plane wave expansion coefficients of the Bloch factors. The latter are determined for statistical ensembles of disordered SiGe alloys using a combination of an empirical pseudopotential model and an extended virtual crystal approximation, whereby the alloy disorder induces the desired symmetry breaking. This approach is in principle very plausible, but a subsequent analysis shows that the corresponding statistical distribution of the valley splitting implied by this method does not lead to a Rice distribution (as observed in experiments and atomistic simulations). Instead, a significantly more skewed distribution is found, which

has a significantly larger probability density at low valley splittings compared to the Rice distribution. Furthermore, in the model by Feng & Joynt, the distribution of the intervalley coupling parameter in the complex plane takes a strongly elliptical shape, which is very different from the nearly circular distribution obtained here (see Appendix C 1). Another consequence of the symmetry-breaking mechanism proposed there is that the variance of the valley splitting in the long-period wiggles-well becomes very large. Thus, the valley splitting enhancement due to the long-period wiggles-well is found to be primarily disorder-dominated and is by no means deterministic. This is reasonable when one assumes that the symmetry breaking is disorder-induced. These predictions on the characteristics of the long-period wiggles-well are in sharp contrast to those obtained in the present work, where the nonsymmorphic screw symmetry is broken via shear strain. As a consequence, the present model predicts a strong deterministic enhancement of the valley splitting in the long-period wiggles-well. The actual microscopic symmetry-breaking mechanism, however, is very likely a combination of both effects. The impact of disorder on the long-period wiggles-well might therefore require further investigation. Finally, the model by Feng & Joynt shows another pronounced resonance for a wiggles-well with intermediate wave number $q = k_0$. In our model, we found that this is caused by a harmonic similar to the configuration described in Sec. III B 4. For typical SiGe parameters (recall that Feng & Joynt used a conduction band offset more typical for Si-MOS), however, the small deterministic resonance is entirely obscured by the disorder-induced component. Therefore, no peak can be observed in the mean valley splitting in Fig. 4.

Finally, we discuss the relation between the present work and the recent paper by Woods *et al.* [33]. In Ref. [33], the shear strain induced symmetry-breaking mechanism to unlock the resonance behind the long-period wiggles-well has been studied for the first time. The envelope function model presented there, which is derived from a one-dimensional tight-binding model, features an intervalley coupling matrix element with unconventional functional form that is notably different from other expressions in the literature. In the present model described in Sec. II of this work, however, the standard form of the intervalley matrix element is preserved even in the presence of strain effects. The numerical results obtained here are qualitatively in an excellent agreement with those reported by Woods *et al.*. In particular the joint linear dependence of the long-period wiggles-well on shear strain and Ge concentration is recovered using the empirical pseudopotential model. Furthermore, we also find good quantitative agreements in the magnitude of the obtained valley splittings. The quantitative comparison, however, requires caution, as the present model also contains disorder-induced contributions, which are omitted in Ref. [33].

V. CONCLUSIONS AND OUTLOOK

We have developed a comprehensive theoretical model that describes a broad range of physical mechanisms determining the valley splitting in Si/SiGe heterostructures, namely alloy-disorder, strain and resonances between valley states across neighboring Brillouin zones. The numerical results are consistent with previously known results but also offer new insights extending the state of the art. With regard to applications, the key accomplishment of the model presented here is a comprehensive characterization of the long-period wobble-well. This includes complex phenomena such as the shear strain-induced symmetry breaking, which unlocks the corresponding resonance mechanism, as well as a quantification of the statistical fluctuations of the valley splitting caused by alloy disorder. Our model predicts a significant deterministic enhancement of the valley splitting for the long-period wobble-well. Due to the critical role of shear strain, we conclude that strain engineering [33, 43, 58] must be further advanced to enhance the design of Si/SiGe spin-qubits.

In contrast to detailed atomistic models, the present model offers a comprehensive description of multiple physical phenomena at very low computational cost. Therefore, it is well suited to rapidly characterize the valley splittings of a vast number of different epitaxial designs. In a subsequent work, the present model will be employed for free-shape optimization of the epitaxial profile to further enhance the valley splitting beyond the simple heuristics considered here.

ACKNOWLEDGMENTS

This work was funded by the Deutsche Forschungsgemeinschaft (DFG, German Research Foundation) under Germany's Excellence Strategy – The Berlin Mathematics Research Center MATH+ (EXC-2046/1, project ID: 390685689, project AA2–17). M. K. is grateful for valuable discussions with Mark Friesen, Merritt P. Losert and Lars R. Schreiber.

Appendix A: Derivation of the Multi-Valley Coupled Envelope Equation Model

In this section, we provide a derivation of the coupled envelope equations (1) loosely following Ref. [66].

We consider the stationary Schrödinger equation for an electronic state in the Si/SiGe heterostructure

$$H(\mathbf{r})\Psi_n(\mathbf{r}) = E_n\Psi_n(\mathbf{r}). \quad (\text{A1})$$

The full Hamiltonian reads

$$H(\mathbf{r}) = H_{\text{cr}}(\mathbf{r}) + U(\mathbf{r}), \quad (\text{A2})$$

which includes the lattice-periodic crystal Hamiltonian

$$H_{\text{cr}}(\mathbf{r}) = -\frac{\hbar^2}{2m_0}\nabla^2 + V_0(\mathbf{r}) \quad (\text{A3})$$

and the confinement potential $U(\mathbf{r})$ described in Eq. (4). Here, m_0 is the vacuum electron mass and $V_0(\mathbf{r})$ is the lattice-periodic potential of the crystal. The crystal potential is invariant under translations with lattice vectors $V_0(\mathbf{r}) \equiv V_0(\mathbf{r} + \mathbf{R}_j)$. We assume that V_0 describes solely the perfectly periodic Si crystal, whereas the effects of Ge in both the QW and the barrier are described by the heterostructure potential that is part of $U(\mathbf{r})$, see Eq. (4). In this way, double-counting of Ge atoms is avoided and alloy disorder effects are separated from the idealized band structure computation.

The translation-invariant lattice-periodic part is solved by Bloch functions that are indexed by a band index n and the wave vector \mathbf{k} as

$$H_{\text{cr}}(\mathbf{r})\phi_{n,\mathbf{k}}(\mathbf{r}) = E_{n,\mathbf{k}}\phi_{n,\mathbf{k}}(\mathbf{r}). \quad (\text{A4})$$

The Bloch function reads

$$\phi_{n,\mathbf{k}}(\mathbf{r}) = \frac{1}{\sqrt{V}}e^{i\mathbf{k}\cdot\mathbf{r}}u_{n,\mathbf{k}}(\mathbf{r}), \quad (\text{A5})$$

where $u_{n,\mathbf{k}}(\mathbf{r}) \equiv u_{n,\mathbf{k}}(\mathbf{r} + \mathbf{R}_j)$ is the lattice-periodic Bloch factor and V is the crystal volume. The Bloch functions form a complete orthonormal basis

$$\int_V d^3r \phi_{n,\mathbf{k}}^*(\mathbf{r})\phi_{n',\mathbf{k}'}(\mathbf{r}) = \delta_{n,n'}\delta_{\mathbf{k},\mathbf{k}'} \quad (\text{A6})$$

and the Bloch factors obey an orthogonality relation for identical wave vectors

$$\frac{1}{\Omega_p} \int_{\Omega_p} d^3r u_{n,\mathbf{k}}^*(\mathbf{r})u_{n',\mathbf{k}}(\mathbf{r}) = \delta_{n,n'}, \quad (\text{A7})$$

where Ω_p is the volume of the primitive unit cell. We assume $V = N\Omega_p$ with N unit cells.

In the presence of the heterostructure, the translation invariance is broken such that the wave vector is not a good quantum number anymore. Therefore, we choose the ansatz

$$\Psi_n(\mathbf{r}) = \sqrt{V} \sum_{\mathbf{k}} F_{n,\mathbf{k}}\phi_{n,\mathbf{k}}(\mathbf{r}), \quad (\text{A8})$$

where $F_{n,\mathbf{k}}$ are expansion coefficients, whose Fourier transform will lead to the envelope wave functions below. We assume normalization of the expansion coefficients

$$V \sum_{\mathbf{k}} |F_{n,\mathbf{k}}|^2 = 1 \quad (\text{A9})$$

to ensure orthonormalization of the full wave function.

In order to construct the multi-valley envelope equation, the expansion coefficients have to be separated into contributions from different valleys. We assume that the coefficients are only non-zero in the vicinity of the valley minima $\mathbf{k} \approx \mathbf{k}_\nu$ such that, following Ref. [66], the expansion coefficient is written as

$$F_{n,\mathbf{k}} = \sum_{\nu} \alpha_{\nu} F_{n,\nu}(\mathbf{k} - \mathbf{k}_\nu) \quad (\text{A10})$$

where ν is the valley-index and α_{ν} is a symmetry factor. We assume normalization as $\sum_{\nu} |\alpha_{\nu}|^2 = 1$.

Following Ref. [66], a Shindo–Nara-type multi-valley coupled envelope equation model is obtained by taking the mean of Eq. (A1) with respect to the ansatz (A8).

1. Lattice-Periodic Part

The lattice-periodic part of the coupled envelope equations is obtained from

$$\begin{aligned} \sum_{n'} \langle \Psi_n | (\hat{H}_{\text{cr}} - E_{n'}) | \Psi_{n'} \rangle &= \\ &= V \sum_{n'} \sum_{\mathbf{k}, \mathbf{k}'} F_{n, \mathbf{k}}^* F_{n', \mathbf{k}'} \times \\ &\quad \times \int d^3 r \phi_{n, \mathbf{k}}^*(\mathbf{r}) (H_{\text{cr}}(\mathbf{r}) - E_{n'}) \phi_{n', \mathbf{k}'}(\mathbf{r}) \\ &= V \sum_{\mathbf{k}} (E_{n, \mathbf{k}} - E_n) |F_{n, \mathbf{k}}|^2, \end{aligned}$$

where we used Eqs. (A4) and (A6). Using the valley-separation (A10) and the parabolic band approximation

$$E_{n, \mathbf{k}_\nu + \mathbf{k}} \approx E_{n, \mathbf{k}_\nu} + \frac{\hbar^2}{2} \mathbf{k} \cdot m_{n, \mathbf{k}_\nu}^{-1} \mathbf{k}, \quad (\text{A11})$$

one arrives at

$$\begin{aligned} \sum_{n'} \langle \Psi_n | \hat{H}_{\text{cr}} | \Psi_{n'} \rangle &= V \sum_{\nu} |\alpha_\nu|^2 \sum_{\mathbf{k}} F_{n, \nu}^*(\mathbf{k}) \times \\ &\quad \times \left(E_{n, \mathbf{k}_\nu} - E_n + \frac{\hbar^2}{2} \mathbf{k} \cdot m_{n, \mathbf{k}_\nu}^{-1} \mathbf{k} \right) F_{n, \nu}(\mathbf{k}), \end{aligned}$$

where we used the strong localization of the valley-envelopes in reciprocal space such that

$$F_{n, \nu'}(\mathbf{k} + \mathbf{k}_\nu - \mathbf{k}_{\nu'}) \approx \delta_{\nu, \nu'} F_{n, \nu}(\mathbf{k}).$$

Finally, inverse Fourier transform

$$F_{n, \nu}(\mathbf{k}) = \frac{1}{V} \int_V d^3 r e^{-i\mathbf{k} \cdot \mathbf{r}} F_{n, \nu}(\mathbf{r}) \quad (\text{A12})$$

and integration by parts yields

$$\begin{aligned} \sum_{n'} \langle \Psi_n | \hat{H}_{\text{cr}} | \Psi_{n'} \rangle &= \\ &= \sum_{\nu} |\alpha_\nu|^2 \frac{\hbar^2}{2} \mathbf{n} \cdot m_{n, \mathbf{k}_\nu}^{-1} \left(F_{n, \nu}^*(\mathbf{r}) \nabla F_{n, \nu}(\mathbf{r}) - \right. \\ &\quad \left. - F_{n, \nu}(\mathbf{r}) \nabla F_{n, \nu}^*(\mathbf{r}) \right) \Big|_{\partial V} \\ &\quad + \sum_{\nu} |\alpha_\nu|^2 \int_V d^3 r F_{n, \nu}^*(\mathbf{r}) \left((E_{n, \mathbf{k}_\nu} - E_n) F_{n, \nu}(\mathbf{r}) \right. \\ &\quad \left. - \frac{\hbar^2}{2} \nabla \cdot (m_{n, \mathbf{k}_\nu}^{-1} \nabla F_{n, \nu}(\mathbf{r})) \right). \end{aligned} \quad (\text{A13})$$

The first term is a boundary condition for the envelope wave functions. The second term includes the band edge energy and the kinetic energy in effective mass approximation for the coupled envelope equation model.

2. Heterostructure Part

In the following, the corresponding computation is carried out for the heterostructure part, which finally yields

a coupling between the different valley-specific envelope wave functions. The ansatz (A8) with (A10) yields

$$\begin{aligned} \sum_{n'} \langle \Psi_n | \hat{U} | \Psi_{n'} \rangle &= \sum_{n'} \sum_{\mathbf{k}, \mathbf{k}'} F_{n, \mathbf{k}}^* F_{n', \mathbf{k}'} \times \\ &\quad \times \int_V d^3 r e^{-i(\mathbf{k} - \mathbf{k}') \cdot \mathbf{r}} U(\mathbf{r}) u_{n, \mathbf{k}}^*(\mathbf{r}) u_{n', \mathbf{k}'}(\mathbf{r}) \\ &= \sum_{n'} \sum_{\mathbf{k}, \mathbf{k}'} \sum_{\nu, \nu'} \alpha_\nu^* \alpha_{\nu'} F_{n, \nu}^*(\mathbf{k}) F_{n', \nu'}(\mathbf{k}') \int_V d^3 r \times \\ &\quad \times e^{-i(\mathbf{k} - \mathbf{k}' + \mathbf{k}_\nu - \mathbf{k}_{\nu'}) \cdot \mathbf{r}} U(\mathbf{r}) u_{n, \mathbf{k}_\nu + \mathbf{k}}^*(\mathbf{r}) u_{n', \mathbf{k}_{\nu'} + \mathbf{k}'}(\mathbf{r}). \end{aligned}$$

The dispersion of the near band-edge Bloch factors is ignored by using the approximation

$$u_{n, \mathbf{k}_\nu + \mathbf{k}}(\mathbf{r}) \approx u_{n, \mathbf{k}_\nu}(\mathbf{r}).$$

With this and the inverse Fourier transform (A12) we arrive at

$$\begin{aligned} \sum_{n'} \langle \Psi_n | \hat{U} | \Psi_{n'} \rangle &\approx \sum_{n'} \sum_{\nu, \nu'} \alpha_\nu^* \alpha_{\nu'} \int_V d^3 r e^{-i(\mathbf{k}_\nu - \mathbf{k}_{\nu'}) \cdot \mathbf{r}} \times \\ &\quad \times F_{n, \nu}^*(\mathbf{r}) F_{n', \nu'}(\mathbf{r}) U(\mathbf{r}) u_{n, \mathbf{k}_\nu}^*(\mathbf{r}) u_{n', \mathbf{k}_{\nu'}}(\mathbf{r}). \end{aligned}$$

This expression is separated into the intravalley ($\nu = \nu'$) and intervalley ($\nu \neq \nu'$) contributions. Since the Bloch factors vary on an atomistic scale, *i.e.*, much faster than the confinement potential and the envelope wave function, the intravalley part is obtained as [67]

$$\begin{aligned} \sum_{n'} \langle \Psi_n | \hat{U} | \Psi_{n'} \rangle \Big|_{\text{intra}} &= \sum_{n'} \sum_{\nu} \alpha_\nu^* \alpha_\nu \int_V d^3 r \times \\ &\quad \times F_{n, \nu}^*(\mathbf{r}) F_{n', \nu}(\mathbf{r}) U(\mathbf{r}) u_{n, \mathbf{k}_\nu}^*(\mathbf{r}) u_{n', \mathbf{k}_\nu}(\mathbf{r}) \\ &\approx \sum_{n'} \sum_{\nu} |\alpha_\nu|^2 \Omega_p \sum_{j=1}^N F_{n, \nu}^*(\mathbf{R}_j) F_{n', \nu}(\mathbf{R}_j) U(\mathbf{R}_j) \\ &\quad \times \frac{1}{\Omega_p} \int_{\Omega_p} d^3 r u_{n, \mathbf{k}_\nu}^*(\mathbf{r}) u_{n', \mathbf{k}_\nu}(\mathbf{r}) \\ &\approx \sum_{\nu} |\alpha_\nu|^2 \int_V d^3 r F_{n, \nu}^*(\mathbf{r}) U(\mathbf{r}) F_{n, \nu}(\mathbf{r}), \end{aligned} \quad (\text{A14})$$

where we used the orthogonality relation (A7). The corresponding intervalley contribution is obtained as

$$\begin{aligned} \sum_{n'} \langle \Psi_n | \hat{U} | \Psi_{n'} \rangle \Big|_{\text{inter}} &\approx \\ &\approx \sum_{n'} \sum_{\nu, \nu' \neq \nu} \alpha_\nu^* \alpha_{\nu'} \sum_{\mathbf{G}, \mathbf{G}'} c_{n, \mathbf{k}_\nu}^*(\mathbf{G}) c_{n', \mathbf{k}_{\nu'}}(\mathbf{G}') \times \\ &\quad \times \int_V d^3 r F_{n, \nu}^*(\mathbf{r}) e^{-i(\mathbf{G} - \mathbf{G}' + \mathbf{k}_\nu - \mathbf{k}_{\nu'}) \cdot \mathbf{r}} U(\mathbf{r}) F_{n', \nu'}(\mathbf{r}). \end{aligned} \quad (\text{A15})$$

where we used a plane wave expansion of the Bloch factors.

3. Coupled Envelopes

The combination of Eqs. (A13)–(A15) yields a system of multi-valley coupled envelope equations

$$\begin{aligned}
E_n F_{n,\nu}(\mathbf{r}) = & -\frac{\hbar^2}{2} \nabla \cdot (m_{n,\mathbf{k}_\nu}^{-1} \nabla F_{n,\nu}(\mathbf{r})) \\
& + (E_{n,\mathbf{k}_\nu} + U(\mathbf{r})) F_{n,\nu}(\mathbf{r}) \\
& + \sum_{n'} \sum_{\nu' \neq \nu} \frac{\alpha_\nu^* \alpha_{\nu'}}{|\alpha_\nu|^2} \sum_{\mathbf{G}, \mathbf{G}'} c_{n,\mathbf{k}_\nu}^*(\mathbf{G}) c_{n',\mathbf{k}_{\nu'}}(\mathbf{G}') \times \\
& \times e^{-i(\mathbf{G}-\mathbf{G}'+\mathbf{k}_\nu-\mathbf{k}_{\nu'}) \cdot \mathbf{r}} U(\mathbf{r}) F_{n',\nu'}(\mathbf{r}).
\end{aligned}$$

In the case of a single band (conduction band only, band indices n, n' are suppressed in the following), two valleys at $\mathbf{k}_\nu = \pm \mathbf{k}_0$, symmetry factors $\alpha_\nu = 1/\sqrt{2}$ and identical effective masses $m_{n,\mathbf{k}_\nu} \equiv m$ and band edge energies $E_{n,\mathbf{k}_\nu} \equiv E_c$, we obtain

$$\begin{pmatrix} H_0(\mathbf{r}) & V_c(\mathbf{r}) \\ V_c^*(\mathbf{r}) & H_0(\mathbf{r}) \end{pmatrix} \begin{pmatrix} F_+(\mathbf{r}) \\ F_-(\mathbf{r}) \end{pmatrix} = E \begin{pmatrix} F_+(\mathbf{r}) \\ F_-(\mathbf{r}) \end{pmatrix}$$

with

$$\begin{aligned}
H_0(\mathbf{r}) &= -\frac{\hbar^2}{2} \nabla \cdot (m^{-1} \nabla) + E_c + U(\mathbf{r}), \\
V_c(\mathbf{r}) &= \sum_{\mathbf{G}, \mathbf{G}'} c_+^*(\mathbf{G}) c_-(\mathbf{G}') e^{-i(\mathbf{G}-\mathbf{G}'+2\mathbf{k}_0) \cdot \mathbf{r}} U(\mathbf{r})
\end{aligned}$$

Renaming $F_\pm(\mathbf{r}) \rightarrow \Psi_\pm(\mathbf{r})$ and ignoring the constant band edge energy E_c finally yields Eq. (1).

Appendix B: Evaluation of Valley Splitting Components and Band Structure Coefficients

In the small strain limit, the reciprocal lattice vectors are written as $\mathbf{G}_n = \sum_{j=1}^3 n_j (I - \varepsilon) \mathbf{b}_j$, where the \mathbf{b}_j are the primitive reciprocal lattice vectors of the relaxed fcc lattice [56]

$$\mathbf{b}_1 = \frac{2\pi}{a_0} \begin{pmatrix} -1 \\ 1 \\ 1 \end{pmatrix}, \quad \mathbf{b}_2 = \frac{2\pi}{a_0} \begin{pmatrix} 1 \\ -1 \\ 1 \end{pmatrix}, \quad \mathbf{b}_3 = \frac{2\pi}{a_0} \begin{pmatrix} 1 \\ 1 \\ -1 \end{pmatrix}.$$

Therefore, the difference between two reciprocal lattice vectors reads

$$\mathbf{G}_n - \mathbf{G}_{n'} = \sum_{j=1}^3 \Delta n_j \mathbf{b}_j^\varepsilon$$

where $\Delta n_j = n_j - n'_j \in \mathbb{Z}$ is an integer and $\mathbf{b}_j^\varepsilon = (I - \varepsilon) \mathbf{b}_j$ is a compact notation for the strained primitive reciprocal lattice vector.

We will now evaluate the contribution to the valley splitting from Eq. (24). Evaluation of Eqs. (25) and (34) is carried out along the same lines. The summation in

Eq. (24) can be rewritten as

$$\begin{aligned}
\Delta_{\text{det}}^l &= \sum_{\Delta n_1} \sum_{\Delta n_2} \sum_{\Delta n_3} \sum_{\mathbf{G}, \mathbf{G}'} c_+^*(\mathbf{G}) c_-(\mathbf{G}') \delta_{\mathbf{G}-\mathbf{G}', \sum_j \Delta n_j \mathbf{b}_j^\varepsilon} \\
&\times e^{-\left(\frac{l_x}{2} \sum_j \Delta n_j \mathbf{e}_x^T \mathbf{b}_j^\varepsilon\right)^2} e^{-\left(\frac{l_y}{2} \sum_j \Delta n_j \mathbf{e}_y^T \mathbf{b}_j^\varepsilon\right)^2} \\
&\times \int dz e^{-i(\sum_j \Delta n_j \mathbf{e}_z^T \mathbf{b}_j^\varepsilon + 2k_0)z} \times \\
&\times (U_{\text{QW}}(z) + U_F(z)) \psi_0^2(z),
\end{aligned}$$

where we have inserted a three-dimensional Kronecker delta and summation with $\Delta n_{i=1,2,3}$ running over all integers. As the in-plane extension of the QD is much larger than the lattice constant $l_x, l_y \gg a_0$, the Gaussian terms (second line) effectively reduce to simple selection rules encoded by new Kronecker delta functions:

$$\begin{aligned}
e^{-\left(\frac{l_x}{2} \sum_j \Delta n_j \mathbf{e}_x^T \mathbf{b}_j^\varepsilon\right)^2} &\approx \delta_{-\Delta n_1 + \Delta n_2 + \Delta n_3, 0} e^{-\left(\frac{l_x}{2} \sum_j \Delta n_j \mathbf{e}_x^T \varepsilon \mathbf{b}_j\right)^2}, \\
e^{-\left(\frac{l_y}{2} \sum_j \Delta n_j \mathbf{e}_y^T \mathbf{b}_j^\varepsilon\right)^2} &\approx \delta_{+\Delta n_1 - \Delta n_2 + \Delta n_3, 0} e^{-\left(\frac{l_y}{2} \sum_j \Delta n_j \mathbf{e}_y^T \varepsilon \mathbf{b}_j\right)^2}.
\end{aligned}$$

These selection rules greatly simplify the evaluation of the summation in Δ_{det}^l , which (after renaming the remaining summation index to n) yields the compact result

$$\Delta_{\text{det}}^l = \sum_{n \in \mathbb{Z}} C_n^{(2)} J_n^l. \quad (\text{B1})$$

Here we have introduced the family of integrals indexed by $n \in \mathbb{Z}$

$$\begin{aligned}
J_n^l &= e^{-\frac{1}{4}(nG_{0,x}l_x)^2} e^{-\frac{1}{4}(nG_{0,y}l_y)^2} \times \\
&\times \int dz e^{-i(nG_{0,z}+2k_0)z} (U_{\text{QW}}(z) + U_F(z)) \psi_0^2(z)
\end{aligned} \quad (\text{B2})$$

and the band structure coefficients

$$C_n^{(2)} = \sum_{\mathbf{G}, \mathbf{G}'} c_+^*(\mathbf{G}) c_-(\mathbf{G}') \delta_{\mathbf{G}-\mathbf{G}', n\mathbf{G}_0}. \quad (\text{B3})$$

Both expressions involve (components of) the displacement vector

$$\mathbf{G}_0 = \mathbf{b}_1^\varepsilon + \mathbf{b}_2^\varepsilon = \frac{4\pi}{a_0} \begin{pmatrix} -\varepsilon_{z,x} \\ -\varepsilon_{y,z} \\ 1 - \varepsilon_{z,z} \end{pmatrix}, \quad (\text{B4})$$

which is the separation of the two low-energy X points in the strained diamond lattice. The vector \mathbf{G}_0 determines both the resonance conditions in Eq. (B2) as well as the selection rule in Eq. (B3). We note that shear strain components $\varepsilon_{z,x}$ and $\varepsilon_{y,z}$ lead to a Gaussian damping in Eq. (B2) and are therefore expected to reduce the magnitude of the valley splitting. The compact form of Eq. (B1) allows for an efficient numerical evaluation, where the double-summation in Eq. (24) was effectively replaced by a single summation over J_n^l (with precomputed $C_n^{(2)}$) for a few integers only.

Along the same lines, we obtain for Eq. (25) and (34)

$$\Delta_{\text{det}}^t = \sum_{n \in \mathbb{Z}} C_n^{(2)} J_n^t \quad (\text{B5})$$

$$\langle |\Delta_{\text{rand}}|^2 \rangle = \sum_{n \in \mathbb{Z}} C_n^{(4)} J_n^{\text{rand}} \quad (\text{B6})$$

with integrals

$$J_n^t = e^{-\frac{1}{4}(nG_{0,x}l_x)^2} e^{-\frac{1}{4}(nG_{0,y}l_y)^2} \times \quad (\text{B7})$$

$$\begin{aligned} & \times \left(\frac{\hbar\omega_x}{4} \left[1 - \left(\frac{nG_{0,x}l_x}{\sqrt{2}} \right)^2 \right] \right. \\ & \quad \left. + \frac{\hbar\omega_y}{4} \left[1 - \left(\frac{nG_{0,y}l_y}{\sqrt{2}} \right)^2 \right] \right) \\ & \times \int dz e^{-i(nG_{0,z}+2k_0)z} \psi_0^2(z) \\ J_n^{\text{rand}} &= e^{-\frac{1}{8}(nG_{0,x}l_x)^2} e^{-\frac{1}{8}(nG_{0,y}l_y)^2} \frac{(\Delta E_c)^2 \Omega_a}{2\pi l_x l_y} \times \quad (\text{B8}) \\ & \times \int dz e^{-inG_{0,z}z} X(z) (1-X(z)) \psi_0^4(z) \end{aligned}$$

and a second set of band structure coefficients governing the magnitude of the disorder-induced contribution

$$\begin{aligned} C_n^{(4)} &= \sum_{\mathbf{G}, \mathbf{G}'} \sum_{\mathbf{K}, \mathbf{K}'} c_+^*(\mathbf{G}) c_- (\mathbf{G}') c_+ (\mathbf{K}) c_-^* (\mathbf{K}') \times \\ & \times \delta_{\mathbf{G}-\mathbf{G}'-\mathbf{K}+\mathbf{K}', n\mathbf{G}_0}. \end{aligned} \quad (\text{B9})$$

Note that because of the symmetries $J_{-n}^{\text{rand}} = (J_n^{\text{rand}})^*$ and $C_{-n}^{(4)} = (C_n^{(4)})^*$, the summation in Eq. (B6) can be further reduced to

$$\langle |\Delta_{\text{rand}}|^2 \rangle = C_0^{(4)} J_0^{\text{rand}} + 2 \sum_{n=1}^{\infty} \text{Re} (C_n^{(4)} J_n^{\text{rand}}).$$

Finally, we combine the two deterministic contributions (B2) and (B7) into a single expression as

$$J_n^{\text{det}} = J_n^{\text{det},t} + J_n^{\text{det},l}. \quad (\text{B10})$$

Appendix C: Statistics

In this section, we derive the statistical properties of the intervalley coupling parameter Δ and the valley splitting E_{VS} induced by the random alloy disorder.

1. Intervalley Coupling Parameter

We consider the random component of the intervalley coupling parameter given in Eq. (32) and seek for a characterization of its statistical properties in terms of its characteristic function. The characteristic function is the Fourier transform of the probability density function, which is given for a complex-valued variable as

$$\varphi_{\Delta_{\text{rand}}} (s \in \mathbb{C}) = \langle e^{i\text{Re}(s^* \Delta_{\text{rand}})} \rangle.$$

Substitution of Eq. (32) and Eq. (7) yields

$$\varphi_{\Delta_{\text{rand}}} (s \in \mathbb{C}) = \langle e^{i \sum_j \text{Re}(s^* w_j) (N_j - X(\mathbf{R}_j))} \rangle,$$

where we have introduced the shorthand notation

$$w_j = \Delta E_c \Omega_a \sum_{\mathbf{G}, \mathbf{G}'} c_+^* (\mathbf{G}) c_- (\mathbf{G}') e^{-i(\mathbf{G}-\mathbf{G}'+2\mathbf{k}_0) \cdot \mathbf{R}_j} \Psi_0^2 (\mathbf{R}_j).$$

As the local Ge concentration at different lattice sites is statistically independent, we arrive at

$$\varphi_{\Delta_{\text{rand}}} (s) = \prod_j e^{-i\text{Re}(s^* w_j) X(\mathbf{R}_j)} \langle e^{i\text{Re}(s^* w_j) N_j} \rangle$$

where the product runs over all atomic positions in the crystal. Using the characteristic function of a scaled Bernoulli distribution

$$\langle e^{i\text{Re}(s^* w_j) N_j} \rangle = 1 - X(\mathbf{R}_j) + X(\mathbf{R}_j) e^{i\text{Re}(s^* w_j)}$$

we obtain

$$\begin{aligned} \varphi_{\Delta_{\text{rand}}} (s) &= \prod_j e^{-i\text{Re}(s^* w_j) X(\mathbf{R}_j)} \times \\ & \times \left(1 - X(\mathbf{R}_j) + X(\mathbf{R}_j) e^{i\text{Re}(s^* w_j)} \right). \end{aligned}$$

Expansion to second order in w_j (which is proportional to the atomic volume) yields

$$\begin{aligned} \varphi_{\Delta_{\text{rand}}} (s) &\approx \prod_j \left(1 - \frac{1}{2} X(\mathbf{R}_j) (1 - X(\mathbf{R}_j)) (\text{Re}(s^* w_j))^2 \right) \\ &\approx e^{-\frac{1}{2} \sum_j X(\mathbf{R}_j) (1 - X(\mathbf{R}_j)) (\text{Re}(s^* w_j))^2} \\ &= e^{-\frac{1}{4} |s|^2 \Gamma - \frac{1}{4} \text{Re}(s^* C)}. \end{aligned}$$

This is the characteristic function of a scalar complex-valued normal distribution with covariance Γ and relation parameter (or pseudo-covariance) C . This is essentially the statement of the central limit theorem for complex-valued random variables. Hence

$$\Delta_{\text{rand}} \sim \text{ComplexNormal}(\mu = 0, \Gamma, C),$$

where the covariance reads

$$\begin{aligned} \Gamma &= \sum_j X(\mathbf{R}_j) (1 - X(\mathbf{R}_j)) |w_j|^2 \quad (\text{C1}) \\ &= (\Delta E_c)^2 \Omega_a \sum_{\mathbf{G}, \mathbf{G}'} \sum_{\mathbf{K}, \mathbf{K}'} c_+^* (\mathbf{G}) c_- (\mathbf{G}') c_+ (\mathbf{K}) c_-^* (\mathbf{K}') \\ & \times \int d^3 r X(z) (1 - X(z)) e^{-i(\mathbf{G}-\mathbf{G}'+\mathbf{K}-\mathbf{K}') \cdot \mathbf{r}} \Psi_0^4(\mathbf{r}) \\ &= \langle |\Delta_{\text{rand}}|^2 \rangle \end{aligned}$$

and the relation parameter is

$$\begin{aligned} C &= \sum_j X(\mathbf{R}_j) (1 - X(\mathbf{R}_j)) w_j^2 \quad (\text{C2}) \\ &= (\Delta E_c)^2 \Omega_a \sum_{\mathbf{G}, \mathbf{G}'} \sum_{\mathbf{K}, \mathbf{K}'} c_+^* (\mathbf{G}) c_- (\mathbf{G}') c_+^* (\mathbf{K}) c_- (\mathbf{K}') \\ & \times \int d^3 r X(z) (1 - X(z)) e^{-i(\mathbf{G}-\mathbf{G}'+\mathbf{K}-\mathbf{K}'+4\mathbf{k}_0) \cdot \mathbf{r}} \Psi_0^4(\mathbf{r}) \\ &= \langle \Delta_{\text{rand}}^2 \rangle. \end{aligned}$$

From the above considerations and

$$\begin{aligned}\Gamma &= \langle (\text{Re}(\Delta_{\text{rand}}))^2 \rangle + \langle (\text{Im}(\Delta_{\text{rand}}))^2 \rangle, \\ C &= \langle (\text{Re}(\Delta_{\text{rand}}))^2 \rangle - \langle (\text{Im}(\Delta_{\text{rand}}))^2 \rangle \\ &\quad + 2i\langle \text{Re}(\Delta_{\text{rand}}) \text{Im}(\Delta_{\text{rand}}) \rangle,\end{aligned}$$

we conclude that the real and imaginary parts of Δ_{rand} are in fact weakly correlated and have a slightly different variance:

$$\begin{aligned}\langle (\text{Re}(\Delta_{\text{rand}}))^2 \rangle &= \frac{1}{2}(\Gamma + \text{Re}(C)), \\ \langle (\text{Im}(\Delta_{\text{rand}}))^2 \rangle &= \frac{1}{2}(\Gamma - \text{Re}(C)), \\ \langle \text{Re}(\Delta_{\text{rand}}) \text{Im}(\Delta_{\text{rand}}) \rangle &= \frac{1}{2}\text{Im}(C).\end{aligned}$$

Due to the rapidly oscillating term proportional to $4k_0$ in Eq. (C2), however, the relation parameter C is typically orders of magnitude smaller than the covariance Γ , such that $C \approx 0$ is a good approximation. In this limit, the distribution of Δ_{rand} becomes circularly symmetric in the complex plane. Including the shift due to the deterministic contribution $\Delta_{\text{det}} = |\Delta_{\text{det}}| \exp(i\Theta)$, we finally arrive at

$$\text{Re}(\Delta) \sim \text{Normal}\left(\mu = |\Delta_{\text{det}}| \cos(\Theta), \sigma^2 = \frac{1}{2}\Gamma\right), \quad (\text{C3})$$

$$\text{Im}(\Delta) \sim \text{Normal}\left(\mu = |\Delta_{\text{det}}| \sin(\Theta), \sigma^2 = \frac{1}{2}\Gamma\right). \quad (\text{C4})$$

2. Valley Splitting

The statistical distribution of the valley splitting $E_{\text{VS}} = 2|\Delta|$ is again obtained via computation of its characteristic function. We consider

$$\varphi_{E_{\text{VS}}}(s) = \langle e^{iE_{\text{VS}}s} \rangle = \langle e^{2i|\Delta|s} \rangle.$$

Using the probability density function implied by Eqs. (C3)–(C4) we obtain in polar coordinates

$$\begin{aligned}\varphi_{E_{\text{VS}}}(s) &= \int_0^\infty dR e^{2iRs} \frac{R}{\pi\Gamma} e^{-\frac{R^2 + |\Delta_{\text{det}}|^2}{\Gamma}} \times \\ &\quad \times \int_0^{2\pi} d\theta e^{\frac{2R|\Delta_{\text{det}}|}{\Gamma} \cos(\theta - \Theta)} \\ &= \int_0^\infty d\xi e^{i\xi s} \frac{\xi}{2\Gamma} e^{-\frac{1}{2}\frac{\xi^2 + (2|\Delta_{\text{det}}|)^2}{2\Gamma}} I_0\left(\frac{2|\Delta_{\text{det}}|\xi}{2\Gamma}\right).\end{aligned}$$

The last line is the Fourier transform of the probability density function of the Rice distribution. Hence, the statistical distribution of the valley splitting is

$$E_{\text{VS}} \sim \text{Rice}(\nu = 2|\Delta_{\text{det}}|, \sigma^2 = 2\Gamma).$$

-
- [1] D. Loss and D. P. DiVincenzo, Phys. Rev. A **57**, 120 (1998).
 - [2] F. A. Zwanenburg, A. S. Dzurak, A. Morello, M. Y. Simmons, L. C. L. Hollenberg, G. Klimeck, S. Rogge, S. N. Coppersmith, and M. A. Eriksson, Rev. Mod. Phys. **85**, 961 (2013).
 - [3] G. Burkard, T. D. Ladd, A. Pan, J. M. Nichol, and J. R. Petta, Rev. Mod. Phys. **95**, 025003 (2023).
 - [4] S. Neyens, O. K. Zietz, T. F. Watson, F. Luthi, A. Nethewewala, H. C. George, E. Henry, M. Islam, A. J. Wagner, F. Borjans, E. J. Connors, J. Corrigan, M. J. Curry, D. Keith, R. Kotlyar, L. F. Lampert, M. T. Mądzik, K. Millard, F. A. Mohiyaddin, S. Pellerano, R. Pillarisetty, M. Ramsey, R. Savytskyy, S. Schaal, G. Zheng, J. Ziegler, N. C. Bishop, S. Bojarski, J. Roberts, and J. S. Clarke, Nature **629**, 80 (2024).
 - [5] H. C. George, M. T. Mądzik, E. M. Henry, A. J. Wagner, M. M. Islam, F. Borjans, E. J. Connors, J. Corrigan, M. Curry, M. K. Harper, D. Keith, L. Lampert, F. Luthi, F. A. Mohiyaddin, S. Murcia, R. Nair, R. Nahm, A. Nethewewala, S. Neyens, R. D. Raharjo, C. Rogan, R. Savytskyy, T. F. Watson, J. Ziegler, O. K. Zietz, R. Pillarisetty, N. C. Bishop, S. A. Bojarski, J. Roberts, and J. S. Clarke, , arXiv:2410.16583 (2024).
 - [6] T. Koch, C. Godfrin, V. Adam, J. Ferrero, D. Schroller, N. Glaeser, S. Kubicek, R. Li, R. Loo, S. Massar, G. Simion, D. Wan, K. De Greve, and W. Wernsdorfer, , arXiv:2409.12731 (2024).
 - [7] A. R. Mills, C. R. Guinn, M. J. Gullans, A. J. Sigillito, M. M. Feldman, E. Nielsen, and J. R. Petta, Sci. Adv. **8**, eabn5130 (2022).
 - [8] A. Noiri, K. Takeda, T. Nakajima, T. Kobayashi, A. Sammak, G. Scappucci, and S. Tarucha, Nature **601**, 338 (2022).
 - [9] X. Xue, M. Russ, N. Samkharadze, B. Undseth, A. Sammak, G. Scappucci, and L. M. K. Vandersypen, Nature **601**, 343 (2022).
 - [10] L. M. K. Vandersypen, H. Bluhm, J. S. Clarke, A. S. Dzurak, R. Ishihara, A. Morello, D. J. Reilly, L. R. Schreiber, and M. Veldhorst, npj Quantum Inf. **3**, 34 (2017).
 - [11] M. Künne, A. Willmes, M. Oberländer, C. Gorjaew, J. D. Teske, H. Bhardwaj, M. Beer, E. Kammerloher, R. Otten, I. Seidler, R. Xue, L. R. Schreiber, and H. Bluhm, Nat. Commun. **15**, 4977 (2024).
 - [12] I. Seidler, T. Struck, R. Xue, N. Focke, S. Trellenkamp, H. Bluhm, and L. R. Schreiber, npj Quantum Inf. **8**, 100 (2022).
 - [13] R. Xue, M. Beer, I. Seidler, S. Humpohl, J.-S. Tu, S. Trellenkamp, T. Struck, H. Bluhm, and L. R. Schreiber, Nat. Commun. **15**, 2296 (2024).
 - [14] T. Struck, M. Volmer, L. Visser, T. Offermann, R. Xue, J.-S. Tu, S. Trellenkamp, Ł. Cywiński, H. Bluhm, and L. R. Schreiber, Nat. Commun. **15**, 1325 (2024).
 - [15] M. Friesen, S. Chutia, C. Tahan, and S. N. Coppersmith, Phys. Rev. B **75**, 115318 (2007).

- [16] A. L. Saraiva, M. J. Calderón, X. Hu, S. Das Sarma, and B. Koiller, *Phys. Rev. B* **80**, 081305 (2009).
- [17] A. L. Saraiva, M. J. Calderón, R. B. Capaz, X. Hu, S. Das Sarma, and B. Koiller, *Phys. Rev. B* **84**, 155320 (2011).
- [18] B. Paquelet Wuetz, M. P. Losert, S. Koelling, L. E. A. Stehouwer, A.-M. J. Zwerver, S. G. J. Philips, M. T. Mądzik, X. Xue, G. Zheng, M. Lodari, S. V. Amitonov, N. Samkharadze, A. Sammak, L. M. K. Vandersypen, R. Rahman, S. N. Coppersmith, O. Moutanabbir, M. Friesen, and G. Scappucci, *Nat. Commun.* **13**, 7730 (2022).
- [19] M. P. Losert, M. A. Eriksson, R. Joynt, R. Rahman, G. Scappucci, S. N. Coppersmith, and M. Friesen, *Phys. Rev. B* **108**, 125405 (2023).
- [20] J. R. F. Lima and G. Burkard, *Mater. Quantum Technol.* **3**, 025004 (2023).
- [21] M. G. Borselli, R. S. Ross, A. A. Kiselev, E. T. Croke, K. S. Holabird, P. W. Deelman, L. D. Warren, I. Alvarado-Rodriguez, I. Milosavljevic, F. C. Ku, W. S. Wong, A. E. Schmitz, M. Sokolich, M. F. Gyure, and A. T. Hunter, *Appl. Phys. Lett.* **98**, 123118 (2011).
- [22] S. F. Neyens, R. H. Foote, B. Thorgrimsson, T. J. Knapp, T. McJunkin, L. M. K. Vandersypen, P. Amin, N. K. Thomas, J. S. Clarke, D. E. Savage, M. G. Lagally, M. Friesen, S. N. Coppersmith, and M. A. Eriksson, *Appl. Phys. Lett.* **112**, 243107 (2018).
- [23] A. Hollmann, T. Struck, V. Langrock, A. Schmidbauer, F. Schauer, T. Leonhardt, K. Sawano, H. Riemann, N. V. Abrosimov, D. Bougeard, and L. R. Schreiber, *Phys. Rev. Applied* **13**, 034068 (2020).
- [24] D. Degli Esposti, L. E. A. Stehouwer, O. Gül, N. Samkharadze, C. Déprez, M. Meyer, I. N. Meijer, L. Tryputen, S. Karwal, M. Botifoll, J. Arbiol, S. V. Amitonov, L. M. K. Vandersypen, A. Sammak, M. Veldhorst, and G. Scappucci, *npj Quantum Inf.* **10**, 32 (2024).
- [25] C. H. Yang, A. Rossi, R. Ruskov, N. S. Lai, F. A. Mohiyaddin, S. Lee, C. Tahan, G. Klimeck, A. Morello, and A. S. Dzurak, *Nat. Commun.* **4**, 2069 (2013).
- [26] F. Borjans, D. Zajac, T. Hazard, and J. Petta, *Phys. Rev. Applied* **11**, 044063 (2019).
- [27] M. P. Losert, M. Oberländer, J. D. Teske, M. Volmer, L. R. Schreiber, H. Bluhm, S. Coppersmith, and M. Friesen, *PRX Quantum* **5**, 040322 (2024).
- [28] A. David, A. M. Pazhedath, L. R. Schreiber, T. Calarco, H. Bluhm, and F. Motzoi, , *arXiv:2409.07600* (2024).
- [29] V. Langrock, J. A. Krzywda, N. Focke, I. Seidler, L. R. Schreiber, and Ł. Cywiński, *PRX Quantum* **4**, 020305 (2023).
- [30] M. Volmer, T. Struck, A. Sala, B. Chen, M. Oberländer, T. Offermann, R. Xue, L. Visser, J.-S. Tu, S. Trellenkamp, Ł. Cywiński, H. Bluhm, and L. R. Schreiber, *npj Quantum Inf.* **10**, 61 (2024).
- [31] Y. Feng and R. Joynt, *Phys. Rev. B* **106**, 085304 (2022).
- [32] J. Klos, J. Tröger, J. Keutgen, M. P. Losert, N. V. Abrosimov, J. Knoch, H. Bracht, S. N. Coppersmith, M. Friesen, O. Cojocaru-Mirédin, L. R. Schreiber, and D. Bougeard, *Adv. Sci.* **11**, 2407442 (2024).
- [33] B. D. Woods, H. Soomro, E. S. Joseph, C. C. D. Frink, R. Joynt, M. A. Eriksson, and M. Friesen, *npj Quantum Inf.* **10**, 54 (2024).
- [34] T. McJunkin, B. Harpt, Y. Feng, M. P. Losert, R. Rahman, J. P. Dodson, M. A. Wolfe, D. E. Savage, M. G. Lagally, S. N. Coppersmith, M. Friesen, R. Joynt, and M. A. Eriksson, *Nat. Commun.* **13**, 7777 (2022).
- [35] T. McJunkin, E. R. MacQuarrie, L. Tom, S. F. Neyens, J. P. Dodson, B. Thorgrimsson, J. Corrigan, H. E. Ercan, D. E. Savage, M. G. Lagally, R. Joynt, S. N. Coppersmith, M. Friesen, and M. A. Eriksson, *Phys. Rev. B* **104**, 085406 (2021).
- [36] T. B. Boykin, G. Klimeck, M. A. Eriksson, M. Friesen, S. N. Coppersmith, P. von Allmen, F. Oyafuso, and S. Lee, *Appl. Phys. Lett.* **84**, 115 (2004).
- [37] S. Chutia, S. N. Coppersmith, and M. Friesen, *Phys. Rev. B* **77**, 193311 (2008).
- [38] L. Zhang, J.-W. Luo, A. Saraiva, B. Koiller, and A. Zunger, *Nat. Commun.* **4**, 2396 (2013).
- [39] L. Cvitkovich, *Atomistic Modeling of Si Spin Qubits From First Principles*, phdthesis, TU Vienna (2024).
- [40] A. Hosseinkhani and G. Burkard, *Phys. Rev. Research* **2**, 043180 (2020).
- [41] J. R. F. Lima and G. Burkard, *Phys. Rev. Materials* **8**, 036202 (2024).
- [42] V. Sverdlov, O. Baumgartner, T. Windbacher, and S. Selberherr, in *Future Trends in Microelectronics*, edited by S. Luryi, J. Xu, and A. Zaslavsky (Wiley, 2010) Chap. 24, pp. 281–291.
- [43] V. Sverdlov, *Strain-Induced Effects in Advanced MOS-FETs*, Computational Microelectronics (Springer, Vienna, 2011).
- [44] L. F. Peña, J. C. Koepke, J. H. Dycus, A. Mounce, A. D. Baczewski, N. T. Jacobson, and E. Bussmann, *npj Quantum Inf.* **10**, 33 (2024).
- [45] F. Schäffler, *Semicond. Sci. Technol.* **12**, 1515 (1997).
- [46] C. G. Van de Walle and R. M. Martin, *Phys. Rev. B* **34**, 5621 (1986).
- [47] M. L. Cohen and V. Heine, *Solid State Phys.* **24**, 37 (1970).
- [48] J. R. Chelikowsky and M. L. Cohen, *Phys. Rev. B* **10**, 5095 (1974).
- [49] J. R. Chelikowsky and M. L. Cohen, *Phys. Rev. B* **14**, 556 (1976).
- [50] M. V. Fischetti and J. M. Hgman, in *Monte Carlo Device Simulation*, edited by K. Hess (Springer US, Boston, 1991) Chap. Theory and calculation of the deformation potential electron-phonon scattering rates in semiconductors, pp. 123–160.
- [51] M. V. Fischetti and S. E. Laux, *J. Appl. Phys.* **80**, 2234 (1996).
- [52] M. M. Rieger and P. Vogl, *Phys. Rev. B* **48**, 14276 (1993).
- [53] E. Ungersboeck, S. Dhar, G. Karlowatz, V. Sverdlov, H. Kosina, and S. Selberherr, *IEEE Trans. Electron Devices* **54**, 2183 (2007).
- [54] J. Kim and M. V. Fischetti, *J. Appl. Phys.* **108**, 013710 (2010).
- [55] S. Sant, S. Lodha, U. Ganguly, S. Mahapatra, F. O. Heinz, L. Smith, V. Moroz, and S. Ganguly, *J. Appl. Phys.* **113**, 033708 (2013).
- [56] P. Y. Yu and M. Cardona, *Fundamentals of Semiconductors: Physics and Materials Properties*, Graduate Texts in Physics (Springer, Berlin, Heidelberg, 2010).
- [57] C. Corley-Wiciak, M. Zoellner, I. Zaitsev, K. Anand, E. Zatterin, Y. Yamamoto, A. Corley-Wiciak, F. Reichmann, W. Langheinrich, L. Schreiber, C. Manganelli, M. Virgilio, C. Richter, and G. Capellini, *Phys. Rev. Appl.* **20**, 024056 (2023).
- [58] C. Adelsberger, S. Bosco, J. Klinovaja, and D. Loss, *Phys. Rev. Lett.* **133**, 037001 (2024).

- [59] P. Mooney, Materials Science and Engineering: R: Reports **17**, 105 (1996).
- [60] K.-P. Gradwohl, C.-H. Lu, Y. Liu, C. Richter, T. Boeck, J. Martin, and M. Albrecht, Phys. Status Solidi RRL **17**, 2200398 (2023).
- [61] M. Zaiser and R. Wu, Materials Theory **6**, 4 (2022).
- [62] P.-A. Geslin and D. Rodney, J. Mech. Phys. Solids **153**, 104479 (2021).
- [63] P.-A. Geslin, A. Rida, and D. Rodney, J. Mech. Phys. Solids **153**, 104480 (2021).
- [64] D. Culcer, X. Hu, and S. Das Sarma, Phys. Rev. B **82**, 205315 (2010).
- [65] B. D. Woods, M. A. Eriksson, R. Joynt, and M. Friesen, Phys. Rev. B **107**, 035418 (2023).
- [66] K. Shindo and H. Nara, J. Phys. Soc. Jpn. **40**, 1640 (1976).
- [67] G. Bastard, *Wave mechanics applied to semiconductor heterostructures* (Les Editions de Physique, Les Ulis Cedex, 1988).